SEDIMENTOLOGY the journal of the International Association of Sedimentologists

Sedimentology (2012) **59,** 578–604 doi: 10.1111/j.1365-3091.2011.01267.x

Unique authigenic mineral assemblages reveal different diagenetic histories in two neighbouring cold-water coral mounds on Pen Duick Escarpment, Gulf of Cadiz

HANS PIRLET*,[1], LAURA M. WEHRMANN†,‡, ANNELEEN FOUBERT§, BENJAMIN BRUNNER†, DOMINIQUE BLAMART¶, LIES DE MOL*, DAVID VAN ROOIJ*, JAN DEWANCKELE**, VEERLE CNUDDE**, RUDY SWENNEN§, PHILIPPE DUYCK†† AND JEAN-PIERRE HENRIET*

**Renard Centre of Marine Geology, Department of Geology and Soil Science, Ghent University, Krijgslaan 281 s8, B-9000 Gent, Belgium (E-mail: hans.pirlet@vliz.be)*

†Department of Biogeochemistry, Max Planck Institute for Marine Microbiology, Celsiusstrasse 1, D-28359 Bremen, Germany

‡Coral Reef Ecology Work Group, GeoBio-Center, Ludwig-Maximilians Universität, Richard-Wagner-Strasse 10, D-80333 München, Germany

§Department of Earth and Environmental Sciences, Geology, K.U. Leuven, Celestijnenlaan 200E, B-3001 Heverlee, Belgium

¶Laboratoire des Sciences du Climat et de L'Environnement (LSCE), Unité Mixte CEA/CNRS/UVSQ, Bat 12, Avenue de la Terrasse, F- 91190 Gif-sur-Yvette, France

***Department of Geology and Soil Science – UGCT, Ghent University, Krijgslaan 281 s8, B-9000 Gent, Belgium*

††Department of Radiology and Medical Imagery, Ghent University Hospital, De Pintelaan 185, B-9000 Gent, Belgium

Associate Editor – Bernhard Riegl

ABSTRACT

Alpha Mound and Beta Mound are two cold-water coral mounds, located on the Pen Duick Escarpment in the Gulf of Cadiz amidst the El Arraiche mud volcano field where focused fluid seepage occurs. Despite the proximity of Alpha Mound and Beta Mound, both mounds differ in their assemblage of authigenic minerals. Alpha Mound features dolomite, framboidal pyrite and gypsum, whereas Beta Mound contains a barite layer and predominantly euhedral pyrite. The diagenetic alteration of the sedimentary record of both mounds is strongly influenced by biogeochemical processes occurring at shallow sulphate methane transition zones. The combined sedimentological, petrographic and isotopic analyses of early diagenetic features in gravity cores from Alpha Mound and Beta Mound indicate that the contrast in mineral assemblages between these mounds is caused by differences in fluid and methane fluxes. Alpha Mound appears to be affected by strong fluctuations in the fluid flow, causing shifts in redox boundaries, whereas Beta Mound seems to be a less dynamic system. To a large extent, the diagenetic regimes within cold-water coral mounds on the Pen Duick Escarpment appear to be controlled by fluid and methane fluxes deriving from layers underlying the mounds and forcings like pressure gradients caused by bottom current. However, it also becomes evident that authigenic mineral assemblages are not only very sensitive recorders of the diagenetic history of specific cold-water coral mounds, but also affect diagenetic processes in turn. Dissolution of aragonite,

[1]Present address: Flanders Marine Institute (VLIZ), Innovocean Site, Wandelaarkaai 7, B-8400 Oostende, Belgium.

lithification by precipitation of authigenic minerals and subsequent brecciation of these lithified layers may also exert a control on the advective and diffusive fluid flow within these mounds, providing a feedback mechanism on subsequent diagenetic processes.

Keywords Barite, calcite, cold-water coral mound, dolomite, gypsum, pyrite, sulphate methane transition zone.

INTRODUCTION

Cold-water corals are widespread along the north-east Atlantic continental margin (Roberts *et al.*, 2006). The dominant cold-water corals, *Lophelia pertusa* and *Madrepora oculata,* are known to construct mound-like structures up to 300 m in height in the Rockall Trough and Porcupine Seabight (Henriet *et al.*, 1998; De Mol *et al.*, 2002; Kenyon *et al.*, 2003; van Weering *et al.*, 2003). In 2005, one of these mounds (Challenger Mound, Porcupine Seabight) was drilled to its base during Expedition 307 of the Integrated Ocean Drilling Program (IODP) (Ferdelman *et al.*, 2006; Kano *et al.*, 2007; Foubert & Henriet, 2009). More recently, similar cold-water coral mounds, in a juvenile growth stage, have been discovered in the Gulf of Cadiz on top of escarpments in the close vicinity of mud volcanoes (Fig. 1; Foubert *et al.*, 2008; Wienberg *et al.*, 2009; Van Rooij *et al.*, 2010). These cold-water coral mounds represent excellent natural laboratories to study the early diagenetic and biogeochemical processes which affect cold-water carbonates, given that they are not affected by burial and/or meteoric diagenesis (Foubert & Henriet, 2009). Previous studies indicate that cold-water coral mound sediments represent a specific diagenetic environment with a tight coupling between microbial-mediated organic matter degradation and carbonate mineral diagenesis (Ferdelman *et al.*, 2006; Webster *et al.*, 2008). Wehrmann *et al.* (2009) showed that cold-water coral reef sediments have a low content of organic matter characterized by an elevated degradation state due to a high organic matter turnover by oxic microbial respiration. As a consequence of these low rates of carbon degradation, sediment diagenesis is slow. The preservation state of the aragonitic corals is largely controlled by the presence of reactive iron in the siliciclastic fraction of the sediment, which buffers the sulphide produced during bacterial sulphate reduction (Ferdelman *et al.*, 2006; Wehrmann *et al.*, 2009). In addition, the production of CO_2 during organic matter degradation also affects carbonate diagenesis. This production will essentially lead to a decrease of the carbonate saturation state in the pore water and may, thus, induce carbonate dissolution (Morse, 2003). Furthermore, the intermittent growth of coral mounds with episodes of reduced sedimentation or erosion exerts a strong control on early diagenetic processes as these episodes can relocate redox fronts in the subsurface (Pirlet *et al.*, 2010).

The IODP Expedition 307 revealed that the geochemistry and diagenetic processes within Challenger Mound are not influenced by methane or other hydrocarbons (Ferdelman *et al.*, 2006; Webster *et al.*, 2008). In contrast, anaerobic oxidation of methane (AOM) coupled to sulphate reduction in a shallow sulphate methane transition zone (SMTZ) has been reported in the mounds in the Gulf of Cadiz (Foubert *et al.*, 2008; Maignien *et al.*, 2010; Wehrmann *et al.*, 2010). This microbially mediated process leads to a drastic alteration of the original sediment, resulting in the dissolution and precipitation of carbonates and iron and sulphur-bearing minerals (Maignien *et al.*, 2010; Wehrmann *et al.*, 2010). Wehrmann *et al.* (2010) and Maignien *et al.* (2010) identified a shallow SMTZ in both Alpha Mound and Beta Mound and discussed the impact on sediment diagenesis. Evidence was found for a variable position of the SMTZ in Alpha Mound which was attributed to fluid dynamics (Wehrmann *et al.*, 2010).

This study is built upon the findings of Wehrmann *et al.* (2010) and Maignien *et al.* (2010). An in-depth study of the diagenetic features in the sediment of two neighbouring cold-water coral mounds (Alpha Mound and Beta Mound) in the Gulf of Cadiz is conducted (Fig. 1), using sedimentological, mineralogical, petrological and isotopic analyses. Despite the almost identical oceanographic and sedimentological settings of Alpha Mound and Beta Mound, different assemblages of authigenic minerals are observed. Based on these assemblages a reconstruction of the diagenetic environment is made for both mounds. It is postulated that varying fluid fluxes from underlying layers and pressure gradients, caused by bottom currents, are responsible for the differ-

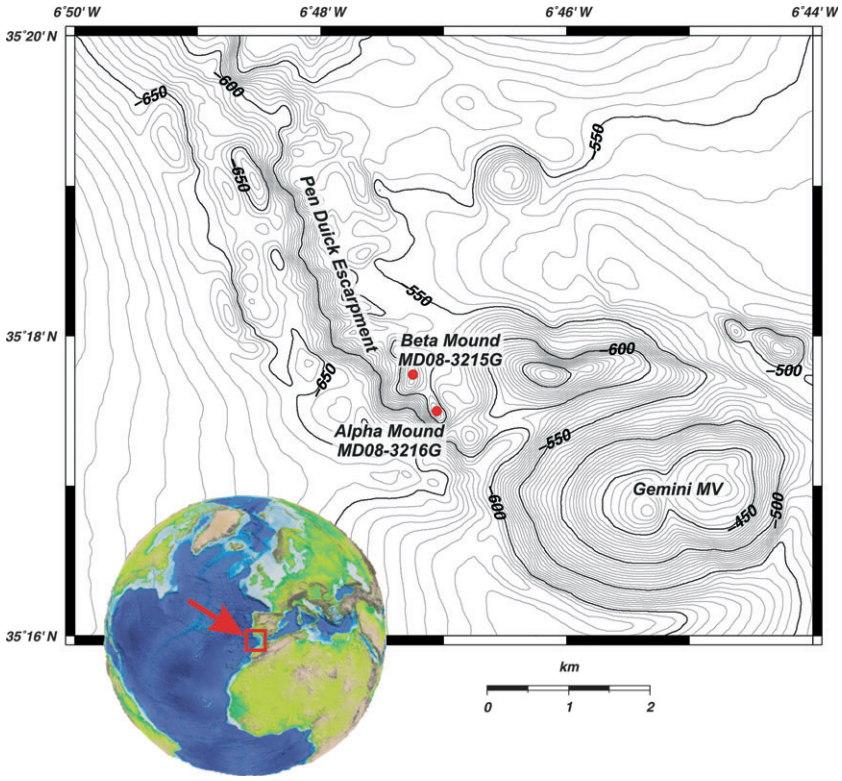

Fig. 1. Bathymetric map of the Pen Duick Escarpment (contour interval every 5 m), off Morocco with the location of the gravity cores retrieved from Alpha Mound (MD08-3216G) and Beta Mound (MD08-3215G; Van Rooij *et al.*, 2010). South-east of the escarpment, the Gemini mud volcano (MV) is indicated.

ent diagenetic history in Alpha Mound and Beta Mound. In addition, the effect of lithification and brecciation processes on the biogeochemical environment is discussed.

Regional setting

The Gulf of Cadiz (Fig. 1) is situated at the front of the Gibraltar Arc, the westernmost tectonic belt of the Alpine–Mediterranean compressional system which has formed by the convergence of the African and Eurasian plates. The geology of this area is extremely complex and is still a matter of debate (Sartori *et al.*, 1994; Maldonado *et al.*, 1999; Gutscher *et al.*, 2002; Zitellini *et al.*, 2009). The westward motion of the front of the Gibraltar Arc caused the Gulf of Cadiz to form as a forearc basin and induced the emplacement of an olistostrome in an accretionary wedge-type depositional environment during the Tortonian (Maldonado *et al.*, 1999; Medialdea *et al.*, 2004). The main part of the olistostrome unit covers the central part of the Gulf of Cadiz as a lobe-shaped structure and extends over 300 km into the Atlantic Ocean (Maldonado *et al.*, 1999; Maestro *et al.*, 2003; Somoza *et al.*, 2003; Medialdea *et al.*, 2004). The end of olistostrome emplacement during the Late Miocene coincides with accelerated tectonic subsidence, while thick progradational and aggradational depositional sequences developed (Maldonado *et al.*, 1999). Plate convergence in the region yields a compressional–transpressional tectonic regime leading to the reactivation of many normal faults and causing mud volcanism and widespread diapirism in the north of the Gulf of Cadiz (Berastegui *et al.*, 1998; Somoza *et al.*, 2003; Pinheiro *et al.*, 2004).

The study area, the El Arraiche mud volcano field, is located on top of the accretionary wedge in water depths between 200 m and 700 m (Van Rensbergen *et al.*, 2005). In this mud volcano field, four cold-water coral mound provinces have been reported which have been named after the steep fault-bounded escarpments and ridges they are located on: (i) the Pen Duick Mound Province; (ii) the Renard Mound Province; (iii) the Vernadsky Mound Province; and (iv) the Al Idrisi Mound Province (Foubert *et al.*, 2008). Alpha Mound and Beta Mound are located on the south-eastern edge of the Pen Duick Escarpment which hosts a total of 15 mounds (Fig. 1). The mounds reach up to 60 m in height, *ca* 500 m in diameter and occur in water depths ranging between 500 m and 600 m (Foubert *et al.*, 2008). Video imagery and surface samples revealed the presence of reef-forming scleractinians, such as *L. pertusa*, *M. oculata* and *Dendrophyllia* sp.; however, few or no living species were observed (Foubert *et al.*, 2008; Van

Rooij *et al.*, 2010; De Mol *et al.*, in press). A more elaborate overview of the temporal and spatial distribution of cold-water corals in the study area is given in Wienberg *et al.* (2009).

Hydrodynamic setting

The hydrodynamic setting in the Gulf of Cadiz is controlled by the exchange of Atlantic and Mediterranean water masses through the Strait of Gibraltar. The upper water mass is the North Atlantic Surface Water (upper 100 m) which, together with the North Atlantic Central Water (100 to 600 m), forms the cool Atlantic Inflow Water into the Mediterranean (Caralp, 1988; Pelegri *et al.*, 2005). Between 600 m and 1500 m water depth two intermediate water masses are observed: Antarctic Intermediate Water from 600 to 900 m and Mediterranean Outflow Water (MOW) below 900 m (Iorga & Lozier, 1999; Pelegri *et al.*, 2005; Machin *et al.*, 2006). Below 1500 m, North Atlantic Deep Water is present. A more elaborate description of the hydrodynamic setting of the study area can be found in Foubert *et al.* (2008) and Van Rooij *et al.* (2010).

MATERIALS AND METHODS

Gravity cores MD08-3215G and MD08-3216G were obtained during the MD-169 MiCROSYSTEMS cruise with *R/V Marion Dufresne* in July 2008. Core MD08-3215G was taken on the top of Beta Mound (35°17·7405′ N and 6°47·2504′ W) and has a length of 343 cm, while MD08-3216G was retrieved from the top of Alpha Mound (35°17·4959′ N and 6°47·0581′ W) and has a total length of 445 cm (Fig. 1). After retrieval both cores were cut into 75 cm sections.

X-ray diffraction analysis

The mineralogical composition of 44 samples of bulk sediment was identified and quantified using X-ray diffraction (XRD) at the Department of Earth and Environmental Sciences, Geology, K.U. Leuven, Belgium [Table 1 (Alpha Mound), Table 2 (Beta Mound)]. First, a representative amount of sediment (*ca* 30 g) was dried before crushing the sample by hand and passing it through a 500 μm sieve. Subsequently, 2·7 g of sample was mixed with 0·3 g ZnO which is added as an internal standard. This mixture was micronized for 5 min in a McCrone Micronizing mill (McCrone Microscopes & Accessories, Westmont, IL, USA) using 4 ml of methanol as lubricating agent. Next, the samples were recuperated in porcelain cups and dried under a fume hood (no extra heating was used). These dried samples were gently disaggregated in a mortar and passed through a 250 μm sieve to ensure good mixing of the sample with the internal standard. Around 0·5 g of powder was needed to fill the sample holders. In order to ensure good packing of the grains back loading was used.

X-ray data were collected on a Philips PW1830 diffractometer (Bragg-Bretano geometry; PANalytical BV, Almelo, The Netherlands) equipped with a CuK radiation source (Generator: 30 mA, 45 kV), graphite monochromator, receiving slit (width: 1 mm), divergence slit (width: 1 mm) and antiscatter slit (width: 0·1 mm). An angular range of 5 to 70° 2θ was measured with a step size of 0·02° and 2 sec counting time, each step. For quantitative phase analysis, the Rietveld refinement program TOPAS ACADEMIC® was used. The quantity of each mineral is expressed as weight percentage.

Petrography

Standard thin sections, embedded in a fluorescent resin, from 15 intervals in Alpha Mound and Beta Mound were manufactured at the Department of Earth and Environmental Sciences, Geology, K.U. Leuven [Table 1 (Alpha Mound), Table 2 (Beta Mound)]. The thin sections were studied using conventional transmitted, reflected and UV light microscopy. A thorough investigation of diagenetic features was conducted with cold cathodoluminescence (CL). In carbonates, CL is routinely used to distinguish chemical and crystallographic zonation, to define paragenetic sequences, to evaluate crystal growth histories and to assess recrystallization of bioclasts and dolomites. It is generally accepted that Mn^{2+} and trivalent REE-ions are the most important activators of extrinsic CL in carbonate minerals, while Fe^{2+} is a quencher of CL (Marshall, 1988; Richter *et al.*, 2003). Therefore, carbonates which precipitated under oxic conditions will normally be non-luminescent while precipitation in a suboxic environment will result in bright-luminescent carbonates (incorporation of Mn^{2+}). Under reducing conditions dull-luminescent carbonates will form (mobilization of Mn^{2+} and Fe^{2+}). In general, calcite is yellow-orange luminescent, while dolomites show orange-red colours. Biogenic carbonate fragments are typically non-luminescent unless they are recrystallized.

Table 1. Overview of the various analyses conducted on core MD08-3216G, Alpha Mound.

Depth (cm)	Thin sections	SEM	Micro-CT scans	Calcite content (%)	Dolomite content (%)	$\delta^{18}O$ (‰ VPDB) bulk carbonate	$\delta^{13}C$ (‰ VPDB) bulk carbonate	CRS (wt.% S)	$\delta^{34}S$-CRS (‰ VCDT)
1				33·5	2·9	−0·30	−1·96		
11								0·53	−18·80
18–20			X						
21				21·4	3·5				
31								1·41	−15·44
51								1·05	−11·46
62–63						1·75	−13·07		
71								0·81	−8·22
81				32·0	13·1				
90–91		X							
91–93	X							0·95	−10·19
101				28·6	11·5				
121				30·2	12·0	0·58	−9·74		
131								0·71	−3·21
141				22·1	16·0				
144–146			X						
151								0·95	−12·74
161				22·0	27·7				
162–164	X								
181				19·0	41·0	4·39	−19·54		
191–193	X							0·88	−10·89
201–202		X		16·6	45·6	4·30	−21·46		
211								0·70	−4·10
219–221			X	17·2	30·3	3·41	−11·50		
231								0·49	−2·91
260–262			X	24·8	25·0				
275–276						3·13	−16·00		
281				26·3	23·3				
289–291	X								
291–292		X						0·85	−7·66
301				24·2	19·0				
311								1·02	−9·99
321–322		X		24·1	23·1	3·01	−13·29		
336–338	X								
341				24·6	19·5				
351								0·91	−13·968

Table 1. (*Continued*)

Depth (cm)	Thin sections	SEM	Micro-CT scans	Calcite content (%)	Dolomite content (%)	$\delta^{18}O$ (‰ VPDB) bulk carbonate	$\delta^{13}C$ (‰ VPDB) bulk carbonate	CRS (wt.% S)	$\delta^{34}S$-CRS (‰ VCDT)
361				26·8	18·4				
365–367	X		X						
371–372		X		47·5	14·5	3·60	−14·58		
381–383			X	27·5	14·2				
401				25·9	12·9	2·77	−8·70		
411								0·56	−5·761
414–416			X						
421				38·8	11·7				
429–431	X								
431–432		X						0·52	−2·956
435–437			X						
441–442		X		44·9	10·8	2·92	−11·08		

Additionally, 14 bulk sediment samples, taken at various depths in the cores from Alpha Mound and Beta Mound [Table 1 (Alpha Mound); Table 2 (Beta Mound)], were disaggregated in distilled water using an ultrasonic bath for 20 sec. Subsequently, the solution was filtered and dried. The filter was gold-coated and studied with a JEOL 6400 scanning electron microscope (SEM; JEOL Limited, Tokyo, Japan) at Ghent University. The composition of several points was analysed using Energy Dispersive Spectroscopy (EDS).

CT scans

Computer tomography (CT) investigates the external and internal structure of objects in three dimensions, in a non-destructive way (Kak & Slaney, 1988). CT scans can be used in coral mound research for the identification and quantification of biogenic fragments and diagenetic features (Foubert & Henriet, 2009; Pirlet *et al.*, 2010). Medical CT scans of the sediment cores were performed with a Siemens medical CT (Medical Imaging Equipment & IT Solutions Sales, Malvern, PA, USA) at Ghent University Hospital (UZ Gent) with an X-ray tube operating at 120 kV and an output of 100 mA. Every 3 mm slices were taken with an overlap of 1 mm. The table feet rotation amounted to 10 mm and the field of view was 150 mm. Furthermore, 14 samples were taken for micro-CT scans in intervals with obvious signs of diagenetic alteration of the sediment [Table 1 (Alpha Mound); Table 2 (Beta Mound)]. The micro-CT scans were conducted at the Centre for X-ray Tomography at Ghent University (UGCT). The set-up of the micro-CT scanner was described in detail by Masschaele *et al.* (2007). A high power directional head was used as an X-ray source. The samples were scanned at 130 kV with a thin Cu-filter, to minimize beam hardening effects. A total of 800 projections were taken, each projection averaging two frames of 400 msec exposure time. A Varian 2520V Paxscan was used as X-ray detector (Varian Medical Systems Inc., Palo Alto, CA, USA).

The CT data were processed with the reconstruction software octopus (UGCT) while 3D morphological analysis was performed using Morpho+ (UGCT). Morpho+ enables the volume to be segmented using advanced thresholding techniques (Vlassenbroeck *et al.*, 2007). Furthermore, it allows different objects to be labelled, classified, quantified and separated in the volume. VGStudioMax 1.2 from Volume Graphics (64 bit version) was used for 3D volume render-

Table 2. Overview of the various analyses conducted on core MD08-3215G, Beta Mound.

Depth (cm)	Thin sections	SEM	Micro-CT scans	Calcite content (%)	Dolomite content (%)	δ^{18}O (‰ VPDB) bulk carbonate	δ^{13}C (‰ VPDB) bulk carbonate	CRS (wt.% S)	δ^{34}S-CRS (‰ VCDT)
1				37·81	2·44	−1·15	−0·90		
3–5	X								
11–12		X							
21				33·01	4·38				
31								0·43	−21·03
41				32·72	3·83				
51								0·53	−14·38
61				29·29	2·60				
68–70			X						
71								0·36	−11·04
79–80						−1·89	−0·73		
81				25·13	4·24				
91								0·55	−0·18
111				48·33	2·72				
115–116		X						0·95	−23·51
116–117						1·13	−2·41		
116–118	X								
121				37·39	2·41				
131								0·51	−12·86
141				31·71	3·06				
161				30·38	4·31				
171								0·89	−7·84
181				32·07	5·11				
199–200						−1·64	−1·73		
201				29·41	5·23				
220–222	X	X		36·32	5·18			0·89	−0·70
241				55·84	3·58				
246–247						2·10	−8·59		
251–252		X						0·72	1·68
254–256	X		X						
261				64·25	2·24				
262–264			X						
271								1·04	−9·25
276–277						−0·68	−2·99		
280–282			X	49·02	1·83				
285–287	X		X	62·08	1·21	2·76	−9·84		
291–292		X						0·44	−4·92
293–295	X								
301				46·49	1·53				
309–311	X		X						
321				41·35	3·07	0·11	−2·71		
331–332		X						0·65	−0·63
Core-catcher	X	X		56·53	1·58			0·56	0·92

ing. During the interpretation of the CT scans special attention was paid to the identification and quantification of diagenetically formed pore space and authigenic minerals.

Stable isotope analyses

Stable carbon (C) and oxygen (O) isotope composition of bulk carbonate

The stable C and O isotope composition was measured for 19 bulk carbonate samples from Alpha Mound and Beta Mound [Table 1 (Alpha Mound); Table 2 (Beta Mound)]. Prior to stable isotope analysis, bulk sediment samples were weighed to ensure an adequate mass of carbonate for isotopic analysis (equivalent to 50 to 70 μg of pure carbonate). All samples were digested in 100% phosphoric acid at 90°C. Samples containing calcite and/or aragonite reacted for 15 min in the acidic bath whereas those with dolomite reacted for 45 min. All isotope analyses were carried out on a VG Optima mass spectrometer (Scientific Instrument Services, Ringoes, NJ, USA) coupled with an automated preparation line at the Laboratoire des Sciences du Climat et de l'Environnement (LSCE, Gif-sur-Yvette, France). All values are reported in per mil relative to Vienna Pee Dee Belemnite (VPDB). Reproducibility is 0·04‰ and 0·05‰, respectively, for the carbon and the oxygen isotope ratios.

Stable C and O isotope composition of extracted dolomite

In the present study, a partial extraction procedure was performed to separate the dolomite fraction from the calcite + aragonite fraction in a sample taken at 181 cm in Alpha Mound. In a first phase, ammonium acetate (1 M) buffered with acetic acid (pH 5) dissolved only calcium carbonate, and to a minor extent the non-stoichiometric dolomite. During a second phase, boiling hydrochloric acid dissolved the rest of the carbonate fraction (stoichiometric dolomite) and possibly also partly some other constituents (clay minerals). Subsequently, stable isotopic measurements were performed at the University of Erlangen (Germany) on the bulk fraction, as well as on separated calcite and dolomite fractions.

Carbonate powders were reacted with 100% phosphoric acid (density >1·9, Wachter & Hayes, 1985) at 75°C using a Kiel III online carbonate preparation line connected to a ThermoFinnigan 252 mass spectrometer (Thermo Fisher Scientific, Waltham, MA, USA). All values are reported in per mil relative to VPDB by assigning a $\delta^{13}C$ value of +1·95‰ and a $\delta^{18}O$ value of −2·20‰ to the National Bureau of Standards (NBS) 19 reference sample. Reproducibility was checked by replicate analysis of laboratory standards. Oxygen isotopic compositions of dolomite were corrected using the fractionation factors given by Rosenbaum & Sheppard (1986). Reproducibility based on laboratory standards was better than ±0·02 for $\delta^{13}C$ (1σ) and ±0·02 for $\delta^{18}O$ (1σ) during this study.

Sulphur (S) isotope composition of chromium reducible sulphur (CRS) fraction

The sulphur isotopic composition of pyrite was measured on 15 samples in Alpha Mound and 15 samples in Beta Mound [Table 1 (Alpha Mound); Table 2 (Beta Mound)]. First, sediment sub-samples were subjected to a two-step chromium-II reduction method (Fossing & Jorgensen, 1989). This method separately traps acid volatile sulphide and CRS as ZnS. The CRS fraction, which mainly consists of sulphur bound as pyrite, was converted into Ag_2S by treatment with $AgNO_3$. Subsequently, precipitates were washed several times with deionized water and dried.

Sulphur isotope ratios were measured by adding 0·4 to 0·6 mg of $BaSO_4$ or 0·2 to 0·4 mg Ag_2S to 1 mg of V_2O_5 in a tin capsule and combusted at 1060°C in an elemental analyzer (EURO EA Elemental Analyzer®; HEKAtech GmbH, Wegberg, Germany) to produce SO_2. The evolved SO_2 was carried by a helium stream through a GC column, Finnigan Conflo III®, and into a Finnigan Delta V® stable isotope ratio mass spectrometer (Thermo Fisher Scientific) to determine the $\delta^{34}S$ value. The sulphur isotope measurements were calibrated with reference materials NBS 127 ($\delta^{34}S$ = +20·3‰) and IAEA-SO-6 ($\delta^{34}S$ = −34·1‰). The standard errors ($\sigma 1$) of the measurements were <0·2‰ for $\delta^{34}S$. The isotope measurements of sulphur are reported with respect to Vienna Canyon Diablo Troilite (VCDT).

Sulphur (S) and oxygen (O) isotope composition of sulphate associated with dolomite

In order to determine the isotope composition of the carbonate-associated sulphate (CAS) in the dolomite, a sequential leaching technique was used. First, the sample (6·7 g) was ground to a grain size smaller than 125 μm. Subsequently, the sample was leached in a 1 M sodium chloride, 0·05 M ascorbic acid solution for 48 h. This leaching step removes easily soluble sulphates (for example, gypsum), whereas the ascorbic acid

inhibits iron oxidation, therefore suppressing oxidation of sulphides (for example, pyrite). The treatment also induces limited dissolution of carbonate, which buffers the ascorbic acid. Next, the sample was centrifuged and the supernatant discarded. The sample was then exposed for 1 h to acetic acid (1·5 M, 50 ml) under a nitrogen atmosphere. This procedural step was chosen to quickly dissolve the entire calcium carbonate fraction, thereby limiting the time for potential oxidation of sulphides by ferric iron released during the acid treatment. The disadvantage of this approach is that also a non-trivial portion of the dolomite fraction is dissolved, thus sulphate trapped in dolomite is partially lost. However, the isotope composition of sulphate in the remaining dolomite fraction is unaltered by this treatment. The residue of this leaching step was recovered by centrifuging, and exposed to concentrated hydrochloric acid for 15 min under a nitrogen atmosphere. The sulphate from the supernatant of this leaching step was recovered by precipitation with barium chloride. Finally, sulphur and oxygen isotopes were measured using a Finnigan Delta V® stable isotope ratio mass spectrometer. The sulphur isotope of CAS is reported with respect to VCDT, the oxygen isotope of CAS is reported with respect to Vienna Standard Mean Ocean Water (V-SMOW).

RESULTS

Lithology and mineralogy

The cores taken on Alpha Mound (MD08-3216G) and Beta Mound (MD08-3215G) contain fragments of *L. pertusa*, *M. oculata*, *Desmophyllum* spp. and *Dendrophyllia* spp. with the density of corals in the sediment ranging between 5% and 30% (Van Rooij *et al.*, 2010). The corals are embedded in a matrix of fine to coarse silt. The sediments in the upper part of both cores are characterized by a brown to greyish brown colour (Alpha Mound: 0 to 9 cm; Beta Mound: 0 to 30 cm) (Figs 2 and 3), while in the lower part, the sediments are grey to olive grey. In Alpha Mound, various lighter levels occur with poorly preserved

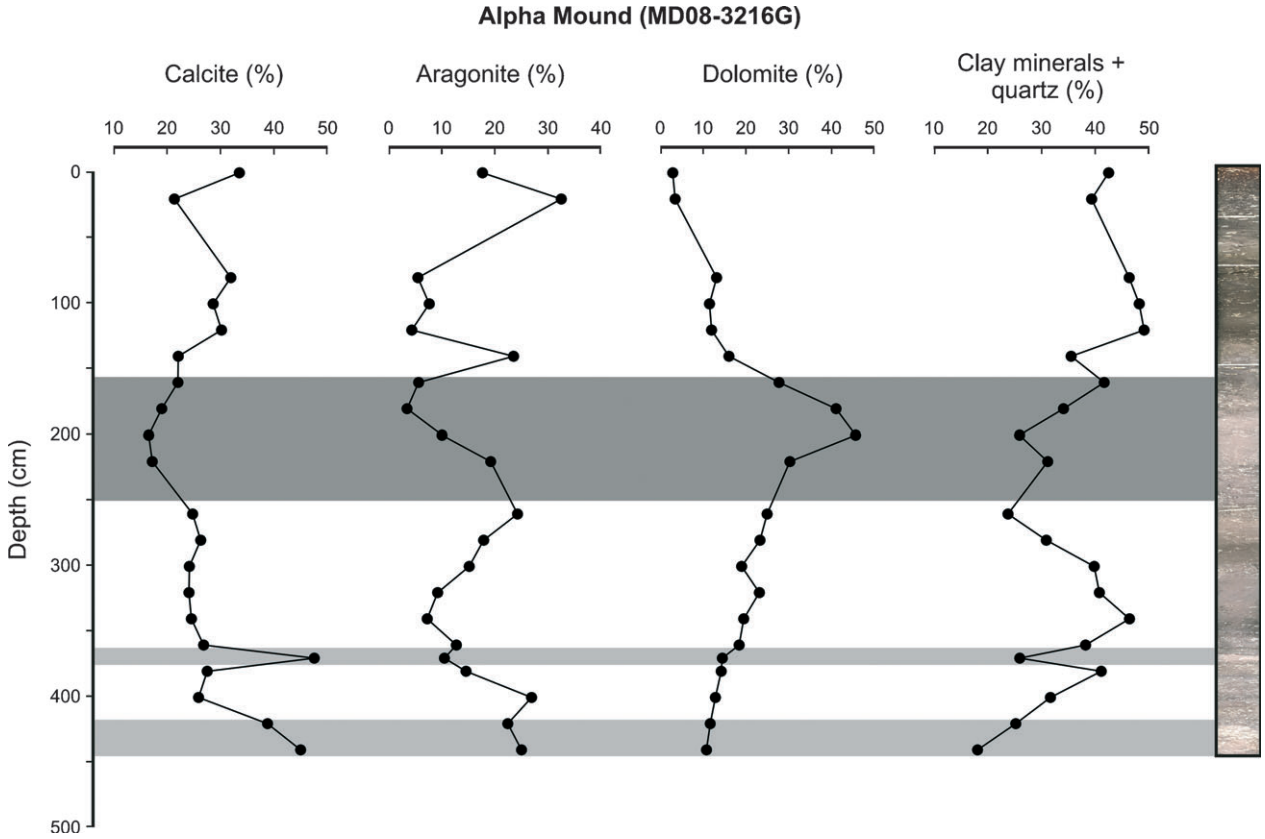

Fig. 2. X-ray diffraction data of the bulk sediment of Alpha Mound (MD08-3216G). The percentages of calcite, aragonite, dolomite and the clay minerals + quartz are indicated and correlated with the core photographs. The lithified layers are indicated in grey.

corals and semi-lithified layers (162 to 255 cm, 367 to 375 cm, 419 to 445 cm). Pale layers with dissolved corals and partial lithification are also present in Beta Mound (101 to 120 cm, 234 to 268 cm, 281 to 300 cm, core catcher).

The dominant mineral in Alpha Mound is calcite with an average content of 27·5% (Fig. 2; Table 1). In the pale, semi-lithified layers in the lower part of the core (367 to 375 cm and 419 to 445 cm), the calcite content increases to 47·5%. High-Ca dolomite (≥40% Ca) constitutes the second most important carbonate mineral with an average content of 18·9% and peaks of 45·6% in the semi-lithified layer at 162 to 255 cm (Fig. 2). This high-Ca dolomite (≥40% Ca) will be referred to as 'dolomite'. The aragonite content varies between 6·0% and 19·0% with an average of 13·2%. Beside the carbonate minerals, quartz (average 13·2%) and clay minerals (average 22·7%) occur (Fig. 2). Clay minerals and quartz co-vary with lower values in the pale, lithified layers and are inversely correlated with the distribution of the carbonate minerals (Fig. 2). Pyrite and feldspar occur in minor quantities in the samples with an average of 0·2% and 2·3% respectively. In the samples taken at 101, 121 and 361 cm, the presence of gypsum was noticed (0·6 to 1·9%).

In Beta Mound, calcite constitutes on average 41·0% of the bulk sediment with peaks up to 62·0% in the pale semi-lithified layers (Fig. 3; Table 2). Aragonite (average 13·5%) is the second most important carbonate mineral, whereas dolomite (average 3·1%) only constitutes a minor fraction of the sediment (Fig. 3). The dolomite distribution correlates with the variations of the clay minerals (average 22·3%) and quartz (average 15·9%) with higher values in between the semi-lithified layers (Fig. 3). Pyrite and feldspar occur in minor quantities in the samples with an average of 0·4% and 3·1%, respectively. In the core catcher, which corresponds to the deepest sediment retrieved from the core, barite constitutes 9·1% of the bulk sediment.

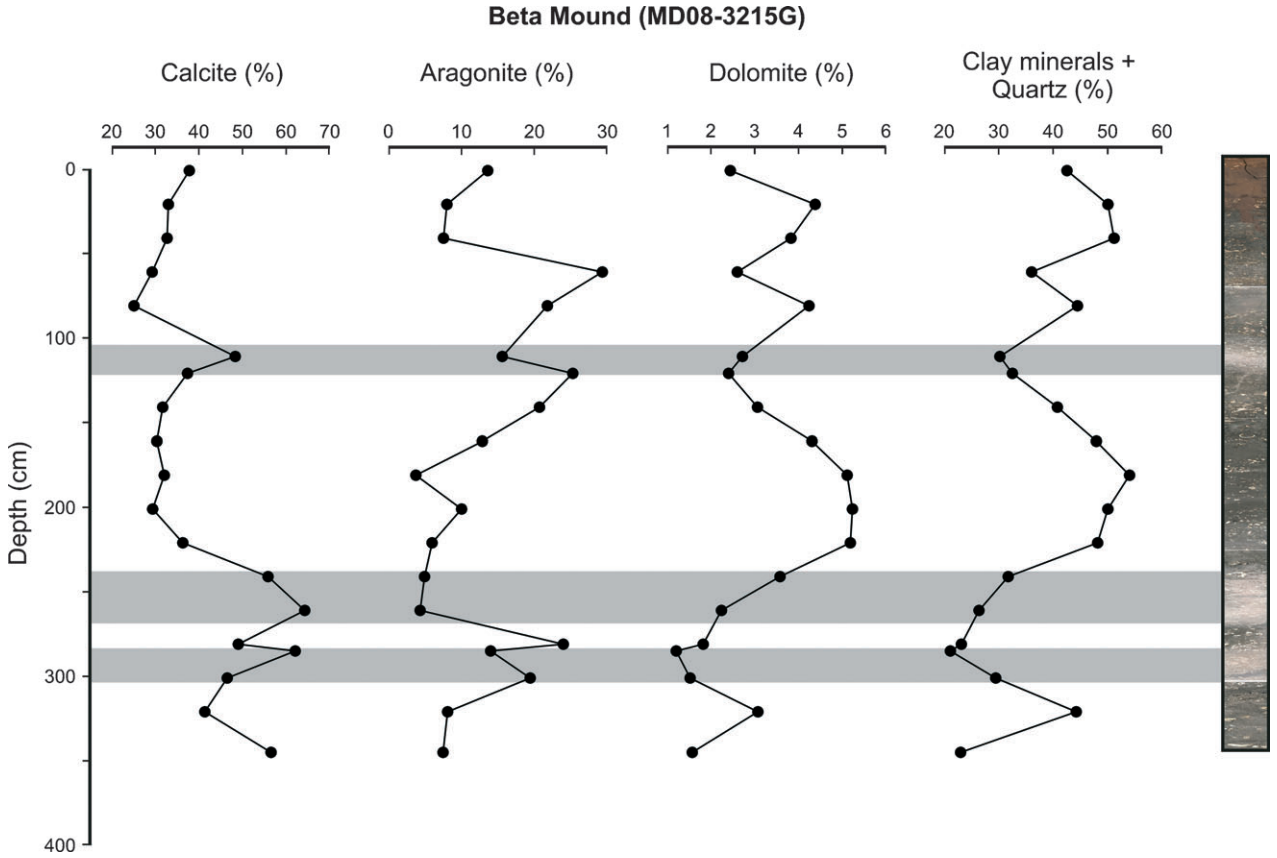

Fig. 3. X-ray diffraction data of the bulk sediment of Beta Mound (MD08-3215G). The percentages of calcite, aragonite, dolomite and the clay minerals + quartz are shown and correlated with the core photographs. The lithified layers are indicated in grey.

Fig. 4. Petrographic observations of Alpha Mound. (A) High concentration of dolomite rhombs at a depth of 201 cm (SEM). (B) Detail of a dolomite crystal incorporating coccoliths and other dolomite rhombs (SEM; 201 to 202 cm). (C) Cold cathodoluminescence (CL) of bright-yellow to orange luminescent dolomite (162 to 164 cm). (D) Cold CL of a zoned dolomite (162 to 164 cm). (E) Intraparticular calcite precipitation in a biogenic fragment (SEM; 431 to 432 cm). (F) Concentration of coarse quartz grains, attributed to a quartz-agglutinating benthic organism (plane-polarized light; 191 to 192 cm). (G) A cluster of framboidal pyrite (reflected light; 91 to 93 cm). (H) Detail of a pyrite framboid (SEM; 291 to 292 cm). (I) A twinned gypsum crystal (white-grey colours), encrusting a coral fragment and incorporating foraminifera (plane-polarized light; 365 to 367 cm). (J) Detail of dolomite rhombs incorporated in the gypsum crystal (SEM; 365 to 367 cm). (K) An EDS profile of the gypsum crystal (365 to 357 cm).

Petrography

In general, the sediment of Alpha Mound consists of micritic carbonate mud with a variable amount of biogenic fragments (foraminifera, corals and undifferentiated shells). Dolomite crystals containing coccoliths and radiolaria were observed in all samples. In the interval between 160 cm and 220 cm a higher concentration of dolomite rhombs (up to 50 μm) was observed in the matrix and in the pores of biogenic fragments; this was confirmed by the observation of rhombohedral crystals under the SEM which were identified as dolomite using EDS (Fig. 4A and B). Cold CL shows bright orange luminescent dolomite crystals with occasional zonation in some of the rhombs (Fig. 4C and D). At depths of 371, 431 and 441 cm calcite overgrowths were observed on coccoliths and in biogenic fragments (Fig. 4E). The thin sections also reveal the presence of feldspar (bright blue luminescent) and quartz grains. In some intervals circular concentrations of coarse quartz grains are observed which are attributed to the presence of a quartz-agglutinating benthic organism (Fig. 4F). Throughout the entire core, clusters of framboidal pyrite were observed in the sediment matrix and in the pores of biogenic fragments (Fig. 4G and H). Between 190 cm and 370 cm the framboids have overgrowths of euhedral pyrite crystals. At a depth of 366 cm, a non-luminescent twinned gypsum crystal (as identified by EDS; Fig. 4K) was observed with a length of *ca* 800 μm (Fig. 4I). This crystal contains small biogenic fragments, dolomite rhombs and encrusts a coral fragment (Fig. 4I and J).

The biogenic fragments of Beta Mound are embedded in a matrix of micritic carbonate mud with quartz and feldspar grains (Fig. 5). In contrast to Alpha Mound, there are no layers containing a significant number of dolomite rhombs. Cold CL reveals the scattered occurrence of small bright-yellow dolomite crystals. In the samples retrieved from a depth of 251 cm and 291 cm and in the core catcher, calcite overgrowth occurs on coccoliths and in the pores of the biogenic fragments (Fig. 5A and B). Throughout the entire core large quantities of euhedral pyrite were found, scattered throughout the sediment matrix or as overgrowths on framboidal pyrite (Fig. 5C to E). In most samples euhedral pyrite is also present in the pores of biogenic fragments and borings in the corals (Fig. 5D and E). Thin sections of the lithified sediment in the core catcher reveal the presence of large quantities of barite which were identified using EDS (Fig. 5F). The barite crystals mostly have dimensions between 50 μm and 100 μm (Fig. 5F to I). The crystals appear in nodules characterized by a sharp transition with the sediment matrix which contains no barite crystals (Fig. 5G). Around and within the barite crystals, euhedral pyrite was observed (Fig. 5I).

CT scans

Both in Alpha Mound (219 to 220 cm and 435 to 437 cm) and Beta Mound (254 to 256 cm, 262 to 264 cm and 285 to 287 cm) various samples with strongly dissolved corals were observed (Fig. 6A to C). In some intervals the corals are completely dissolved and leave mouldic pores in the sediment (Fig. 6D and E). The zones with strongly altered corals coincide with (semi)-lithified intervals. These brittle, (semi)-lithified horizons are more sensitive to fracturing and brecciation (Fig. 6C to E). In most of the samples these secondary fractures are considered an artifact of the sampling process. However, in the samples taken at 435 to 437 cm (Alpha Mound) and 285 to 287 cm (Beta Mound), brecciation is believed to be a genuine feature, since these samples reveal a specific fracture network which is different from that of the other samples. This brecciation can also be noticed in the medical CT scans in Alpha Mound (419 to 445 cm) and Beta Mound (234 to 268 cm and 281 to 300 cm; Fig. 6D and E). The fractures are up to several millimetres wide and, in some cases, are filled with unconsolidated sediment.

Two large pyrite nodules up to 0·7 cm in diameter and containing biogenic fragments were

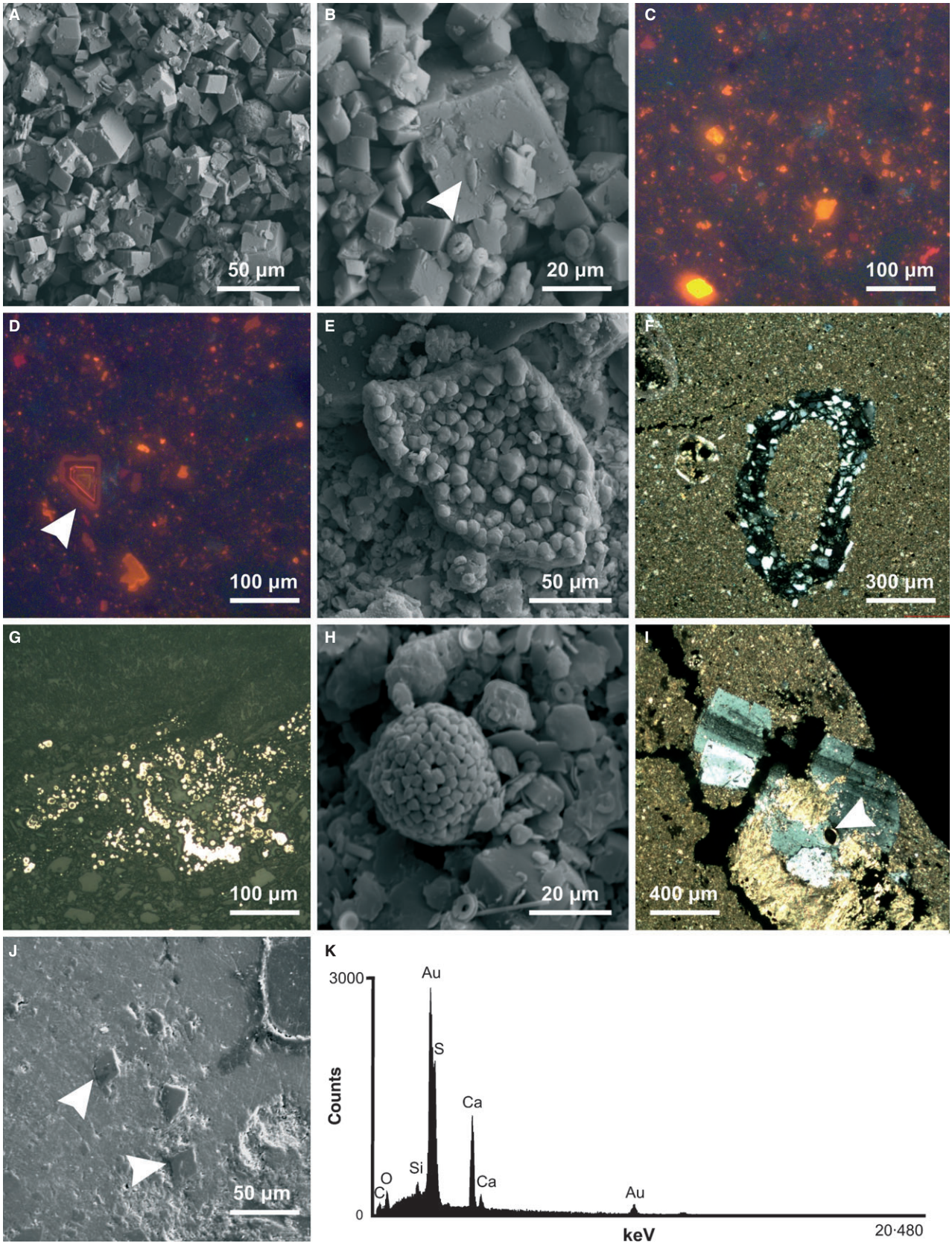
A
50 μm
B
20 μm
C
100 μm
D
100 μm
E
50 μm
F
300 μm
G
100 μm
H
20 μm
I
400 μm
J
50 μm
K
3000
0
Counts
Au
S
Ca
O
C
Si
Ca
Au
keV
20·480

Fig. 6. CT scans. (A) and (B) Micro-CT scans showing the dissolution of corals and the subsequent creation of mouldic porosity in Alpha Mound and Beta Mound (black) (MD08-3216G 219 to 221 cm and MD08-3215 262 to 264 cm). (C) A micro-CT scan of a brecciated (semi)-lithified layer in Beta Mound containing strongly dissolved corals (MD08-3215G 285 to 287 cm). (D) and (E) Medical CT scan of mouldic porosity and brecciation inside a (semi)-lithified layer in Beta Mound. (F) Medical CT scan of pyrite nodules (white) in Beta Mound which precipitate close to coral fragments. (G) A micro-CT scan of a pyrite nodule (yellow) in the sediment matrix (grey) of Beta Mound. (H) A micro-CT scan of pyritized burrows and scattered pyrite (yellow) in the sediment matrix (grey) of Alpha Mound.

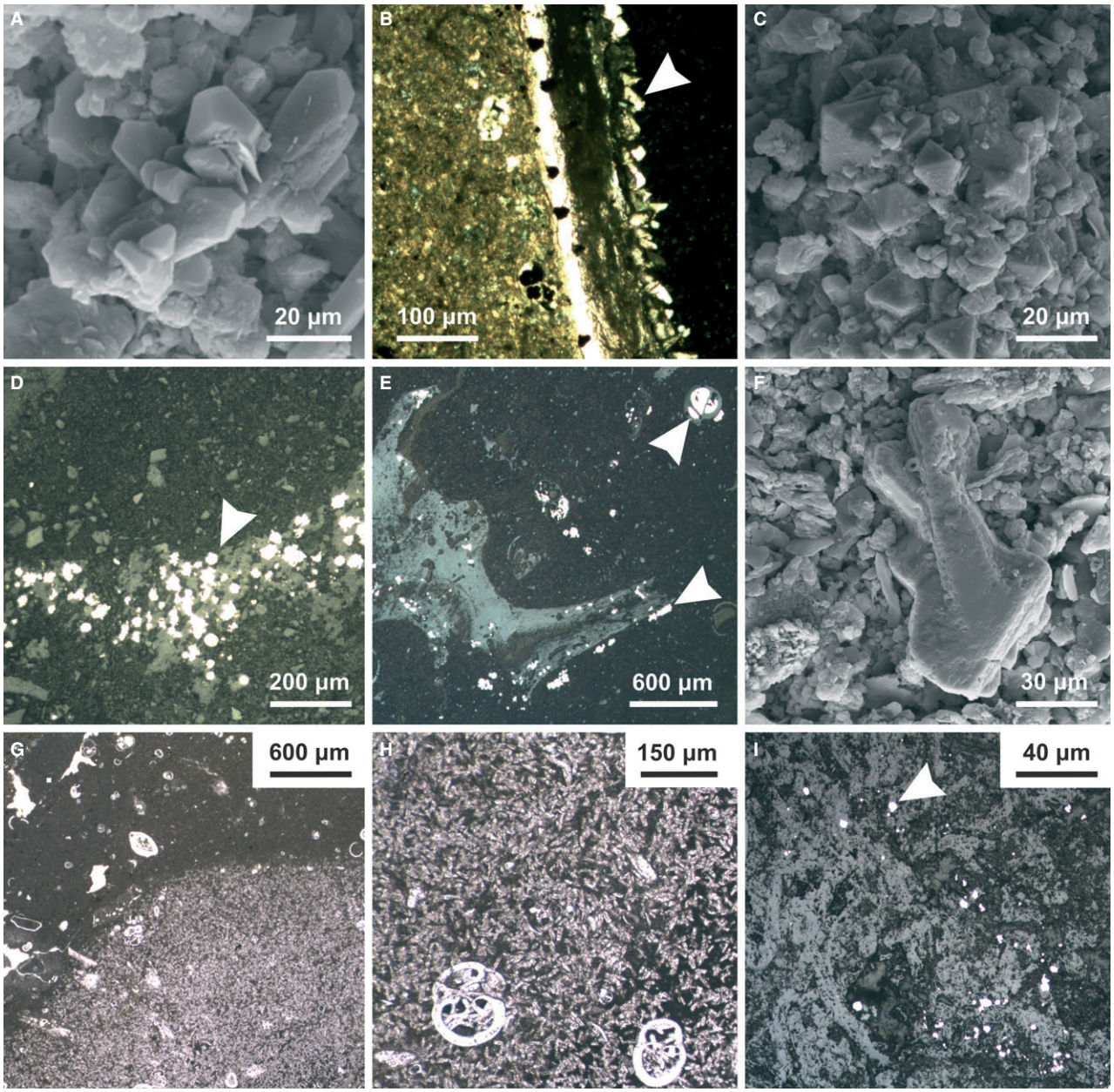

Fig. 5. Petrographic observations of Beta Mound. (A) Calcite crystals (core catcher; SEM). (B) Intraparticular calcite precipitation in the shell of a bivalve (plane-polarized light; 309 to 311 cm). (C) Detail of a cluster of euhedral pyrite (SEM; core catcher). (D) and (E) The precipitation of euhedral pyrite inside biogenic fragments such as corals and foraminifera (reflected light; 116 to 118 and 293 to 295 cm). (F) A twinned barite crystal (SEM; core catcher). (G) The sharp transition between the sediment matrix without barite and the barite nodule (whitish sediment; core catcher). (H) Detail of barite precipitation in the sediment matrix and inside biogenic fragments (core catcher). (I) The presence of euhedral pyrite within and around the barite crystals (reflected light; core catcher).

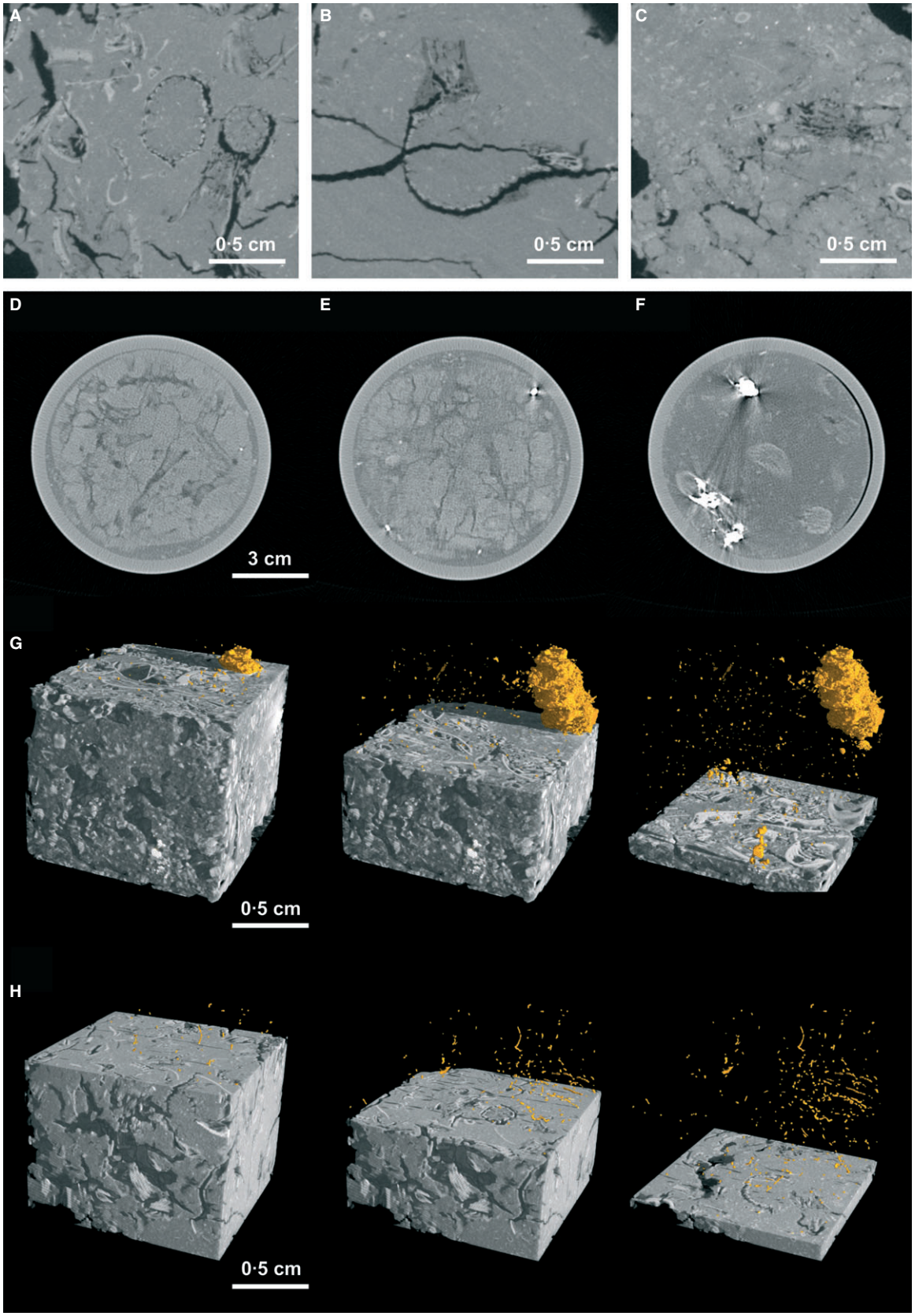
A
0·5 cm
B
0·5 cm
C
0·5 cm
D
E
F
3 cm
G
0·5 cm
H
0·5 cm

observed in the micro-CT of two samples from Beta Mound (309 to 311 cm and 280 to 282 cm, Fig. 6G). In the remaining micro-CT scans of Alpha Mound and Beta Mound sediments only scattered pyrite in the matrix or pyritized burrows were observed (Fig. 6H). However, in the medical CT scans of the entire cores, numerous large pyrite nodules (*ca* 1 cm) were identified in Beta Mound (Fig. 6F) while no nodules were noticed in Alpha Mound. These pyrite nodules occur mostly next to coral fragments.

Stable isotope analyses

The $\delta^{13}C$ and $\delta^{18}O$ values of the bulk carbonate from Alpha Mound and Beta Mound are displayed in Table 1 (Alpha Mound) and Table 2 (Beta Mound). In both mounds, decreases in the $\delta^{13}C$ values of bulk carbonate correspond to an increase in the $\delta^{18}O$ values (Fig. 7A). In Alpha Mound, $\delta^{13}C$ values vary between $-1{\cdot}9‰$ and $-21{\cdot}5‰$, whereas $\delta^{18}O$ values range between $-0{\cdot}3‰$ and $+4{\cdot}4‰$ (Fig. 7B). Except for the surface sample, all samples in Alpha Mound are depleted in ^{13}C and enriched in ^{18}O with respect to VPDB. The lowest $\delta^{13}C$ values are recorded in the semi-lithified and dolomite-rich layers (181 to 201 cm; Fig. 7B). The $\delta^{13}C$ and $\delta^{18}O$ values of the pure dolomite which was extracted from the bulk carbonate in Alpha Mound (181 to 182 cm) are $-22{\cdot}3‰$ and $+4{\cdot}8‰$, respectively (Fig. 7A). The calcite associated with this dolomite has a $\delta^{13}C$ value of $-12{\cdot}5‰$ and a $\delta^{18}O$ value of $+2{\cdot}4‰$ (Fig. 7A). The bulk carbonates of Beta Mound have $\delta^{13}C$ values between $-0{\cdot}7‰$ and $-9{\cdot}8‰$ and $\delta^{18}O$ values between $-1{\cdot}9‰$ and $+2{\cdot}8‰$. A significant drop in $\delta^{13}C$ values and an increase in $\delta^{18}O$ values are observed in the semi-lithified layers of Beta Mound at *ca* 246 cm and 286 cm (Fig. 7B).

Sulphur isotope values of solid phase pyrite ($\delta^{34}S$-CRS) are given in Table 1 (Alpha Mound) and Table 2 (Beta Mound). The sulphur isotope composition of the pyrite phase of Alpha Mound varies between $-18‰$ and $-2{\cdot}9‰$ (Fig. 8). Three intervals with significantly higher $\delta^{34}S$ values can be identified at a depth of 131 cm, 231 cm and 431 cm. In Beta Mound, the $\delta^{34}S$ values for pyrite range between $-23{\cdot}5‰$ and $+1{\cdot}7‰$ (Fig. 8). Three intervals with distinctly heavier isotopic compositions were indentified (91 cm, 251 cm and 345 cm). The $\delta^{34}S$ and $\delta^{18}O_{SMOW}$ value of the CAS from the dolomite phase of a sample with high dolomite content from Alpha Mound (201 cm) is $+21{\cdot}7‰$ and $+12{\cdot}7‰$, respectively.

DISCUSSION

In the following, the different diagenetic phases and features will initially be discussed individually. Subsequently, differences in diagenetic history between Alpha Mound and Beta Mound are discussed and an interpretation in terms of the respective diagenetic environments is proposed.

Sulphur-bearing minerals

Pyrite

The sedimentary pyrite concentration and the sulphur isotopic composition of the pyrite in Alpha Mound and Beta Mound (Fig. 8) are probably the result of a combination of the following processes: (i) hydrogen sulphide production by organoclastic sulphate reduction during organic matter degradation; (ii) hydrogen sulphide production during methanotrophic sulphate reduction [coupled to the anaerobic oxidation of methane (AOM)] in the sulphate methane transition zone (SMTZ) which is diffusing upwards; and (iii) the subsequent reaction of the produced sulphide with reactive iron phases and dissolved iron in the sediment (Berner, 1970; Wehrmann *et al.*, 2010).

Due to their proximity and similar sedimentary setting, Alpha Mound and Beta Mound are assumed to have received a similar amount of reactive iron and organic material. In both mounds, sulphide production by organoclastic and methanotrophic sulphate reduction, albeit a different depth of SMTZ, has led to the almost complete pyritization of reactive mineral phases (Wehrmann *et al.*, 2010). Nevertheless, a distinct shift in the micro-texture of this sedimentary pyrite is observed between Alpha Mound and Beta Mound. Alpha Mound is characterized predominantly by clusters of framboidal pyrite with some minor euhedral overgrowths (Fig. 4G and H), whereas Beta Mound contains large nodules of euhedral pyrite (Figs 5C to E, 6F and G). Framboidal textures are generally assumed to be the result of rapid pyrite formation from aqueous solutions, highly supersaturated with both iron monosulphides and pyrite, in which kinetics favour the formation of iron monosulphides before pyrite (Sweeney & Kaplan, 1973; Raiswell, 1982; Passier *et al.*, 1997, 1999). Euhedral pyrite grows more slowly at saturation levels that are below those of iron monosulphides after *in situ* sources of iron are exhausted and transportation of reactive iron from adjacent sediments is required (Sweeney & Kap-

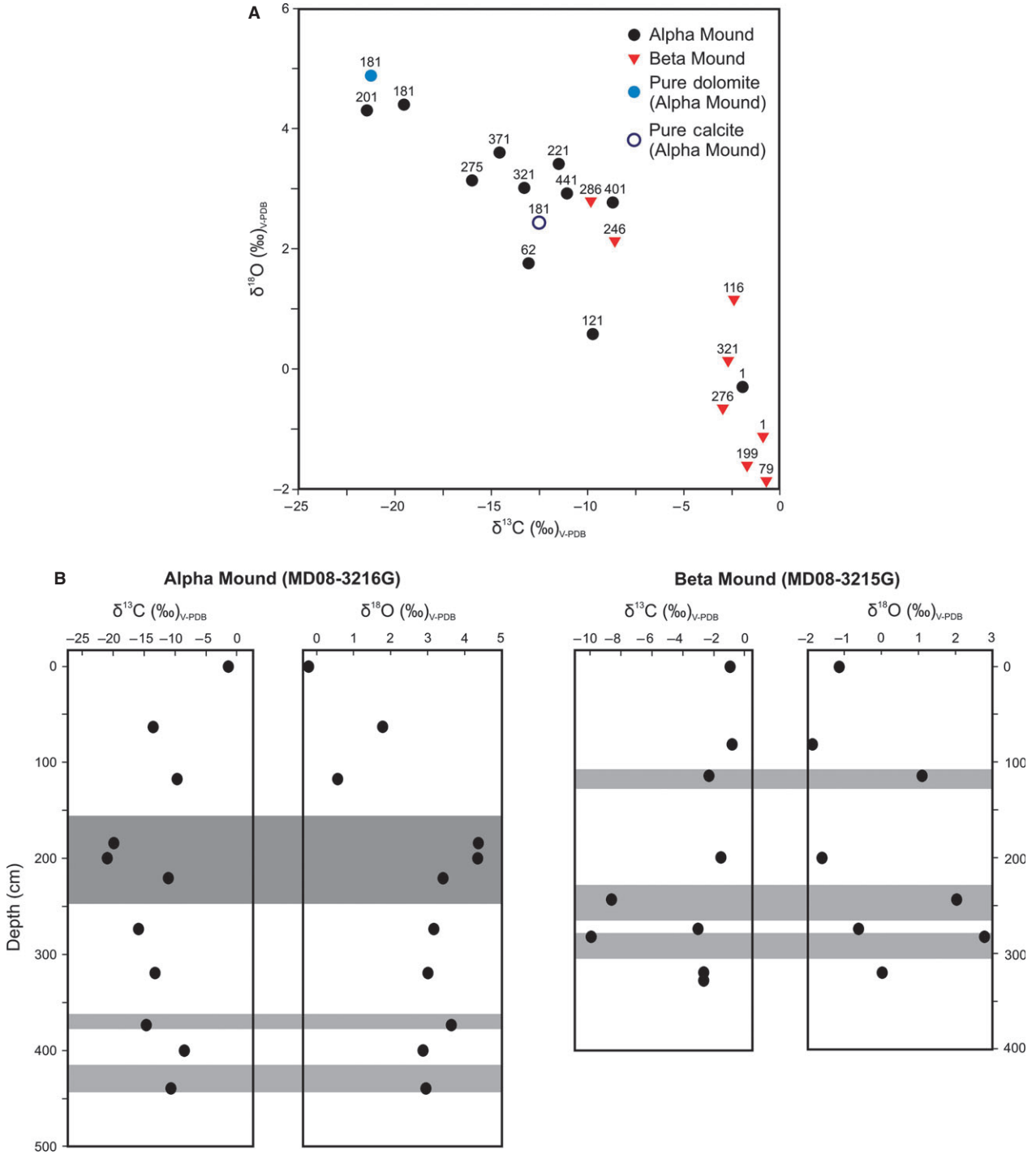

Fig. 7. (A) A plot of the $\delta^{13}C$ versus $\delta^{18}O$ values of the bulk carbonate of Alpha Mound (black dots) and Beta Mound (red triangles). The $\delta^{13}C$ and $\delta^{18}O$ values of the pure dolomite and calcite, both sampled at a depth of 181 cm in Alpha Mound are also shown. (B) The $\delta^{13}C$ and $\delta^{18}O$ values of the bulk carbonate of Alpha Mound and Beta Mound, plotted against depth. The lithified layers are indicated in grey.

lan, 1973; Raiswell, 1982; Passier *et al.*, 1997, 1999). Thus, the shift in pyrite micro-texture indicates that different saturation levels were present in Alpha Mound and Beta Mound. Given that originally a comparable pool of reactive iron was present in both mounds, this difference in saturation level may be attributed to higher hydrogen sulphide concentrations in Alpha Mound compared with Beta Mound (Passier *et al.*, 1999; Ohfuji & Rickard, 2005; Merinero *et al.*, 2008).

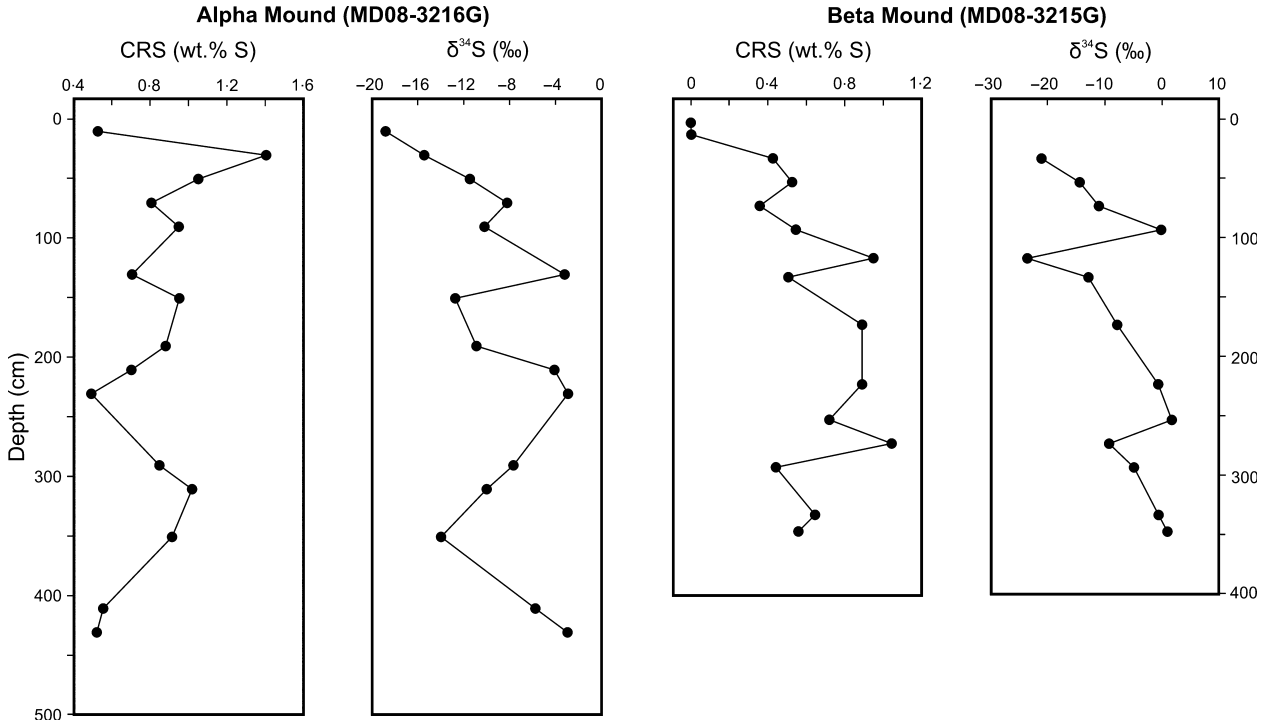

Fig. 8. Weight percentage of the chromium reducible sulphur (CRS; i.e. mostly pyrite) and the δ^{34}S values of the pyrite in Alpha Mound and Beta Mound.

Organoclastic sulphate reduction produces an increase in the δ^{34}S values with depth as the residual pore water sulphate will become progressively enriched in ^{34}S (Goldhaber & Kaplan, 1980). This trend is also reflected in the sulphur isotope composition of sulphide produced by sulphate reduction, explaining general trends to heavier pyrite values with depth. However, both Alpha Mound and Beta Mound contain three zones, characterized by peaks in the δ^{34}S values (Fig. 8). These relatively heavy δ^{34}S values can be attributed to hydrogen sulphide production during sulphate reduction coupled to the AOM which diffuses upwards and overprints the isotopic signature of pyrite formed during organoclastic sulphate reduction (Jørgensen *et al.*, 2004; Neretin *et al.*, 2004). Hence, the zones with higher δ^{34}S values indicate shifts of the SMTZ to shallower depths when compared with the current situation. A similar conclusion was reached by Wehrmann *et al.* (2010).

There is an apparent discrepancy between the differences in the pyrite morphologies of Alpha Mound and Beta Mound (attributed to dissimilar sulphide fluxes), and the similarities in the sulphur isotope patterns (attributed to changes in the SMTZ). It is hypothesized that methane fluxes in Alpha Mound are generally higher, resulting in a shallower SMTZ when compared with Beta Mound. However, the position of the SMTZ in both Alpha Mound and Beta Mound was subjected to relocations as indicated by the positive shifts in the δ^{34}S of pyrite. The latter scenario could explain the apparent mismatch between the pyrite morphologies and the sulphur isotope trends of the two mounds.

Barite

The barite in Beta Mound has a diagenetic origin as it encrusts biogenic fragments and pyrite crystals (Fig. 5F, H and I). Authigenic barite deposits have been documented along numerous continental margins associated with submarine venting of cold fluids enriched in hydrocarbons and barium (Torres *et al.*, 1996, 2003; Dickens, 2001; Greinert *et al.*, 2002; Castellini *et al.*, 2006; Riedinger *et al.*, 2006; Snyder *et al.*, 2007). The barite crystals precipitate above the SMTZ where upward migrating barium-rich, sulphate-depleted fluids react with sulphate-rich pore water (Torres *et al.*, 1996) and, thus, couples the carbon, sulphur and barium cycles (Dickens, 2001; Aloisi *et al.*, 2004). A similar process can be invoked for the formation of barite in Beta Mound at *ca* 345 cm. This is in line with a linear decrease in pore water sulphate concentration observed in a

core that was taken nearby (Wehrmann *et al.*, 2010) which indicates that the current position of the SMTZ is between 350 cm and 450 cm. The source of barium in the barite deposits remains uncertain. Barium could be derived from the dissolution of biogenic barite which is produced in the water column in association with decaying organic matter (Paytan & Griffith, 2007). When pore water gets depleted in sulphate, buried pelagic barite is dissolved, leading to the accumulation of barium in the pore water. However, barium can also be derived from the dissolution of underlying salt deposits and is subsequently transported to the surface by an upward fluid migration (Castellini *et al.*, 2006). The increase of the sodium and chloride concentration in a 1:1 ratio with depth in the pore water of Beta Mound indicates that upward migrating fluids which were affected by evaporite dissolution (Wehrmann *et al.*, 2010) may be the primary source for barium, whereas the dissolution of pelagic barite might act as a secondary contributor. This hypothesis is corroborated by a strong increase in barium concentration with depth in the pore water at the nearby Gemini mud volcano (Hensen *et al.*, 2007). The precipitation of significant amounts of barite (9·1%) in a single layer in Beta Mound indicates that the SMTZ remained stable at a certain depth for a long period which might be related to a period of reduced or even no sedimentation (Torres *et al.*, 1996).

Gypsum

In Alpha Mound, authigenic gypsum crystals were found encrusting corals and dolomite rhombs (Fig. 4I to K). The diagenetic formation of gypsum in a cold-water coral mound was previously reported by Pirlet *et al.* (2010), who concluded that the presence of authigenic gypsum might serve as an indicator for a diagenetic oxidation event. The inflow of sea water is capable of oxidizing iron sulphides, which leads to an acidification of the pore water and causes carbonate dissolution (Ku *et al.*, 1999). Hence, sulphide oxidation induces both sulphate production and an increase in the concentration of calcium in the pore waters due to the dissolution of aragonite; this leads to an oversaturation of the pore water with respect to gypsum (Pirlet *et al.*, 2010). The hypothesis that sporadic sea water inflow occurs in Alpha Mound is supported by the study of Wehrmann *et al.* (2010), who found evidence in the pore water chemistry that such an event recently occurred.

Carbonate minerals

Calcite

Authigenic calcite was observed in various (semi)-lithified intervals in both Alpha Mound and Beta Mound either as intraparticular crystals in biogenic fragments or as overgrowths on coccoliths (Figs 4E, 5A and 5B). The semi-lithified layer, observed in Beta Mound between 101 cm and 120 cm reveals $\delta^{13}C$ and $\delta^{18}O$ values which are close to the values in the 'unaltered' surface samples. Thus, the precipitation of authigenic calcite in this layer may be attributed to early diagenetic processes which are sea water related or driven by organic matter degradation close to the sediment-water interface. Similar lithified layers, characterized by a marine isotopic signature were found in cold-water coral mounds off Ireland and are attributed to carbonate ion diffusion from sea water, supersaturated with respect to calcite, into the pore fluids (Noé *et al.*, 2006).

The negative $\delta^{13}C$ values (around $-10‰$) of the bulk carbonate in the other diagenetic calcite layers of Alpha Mound and Beta Mound (Fig. 7B) suggest that microbially mediated diagenetic processes contributed dissolved inorganic carbon (DIC) which was subsequently incorporated into the calcite cement. Potential sources of DIC are the decay of organic matter and AOM, which can be distinguished by their carbon isotope composition (Curtis *et al.*, 1972; Pisciotto & Mahoney, 1981; Mozley & Burns, 1993; Malone *et al.*, 1994). Microbial degradation of organic matter not only produces DIC, but can also favour or inhibit carbonate precipitation. For example, organoclastic sulphate reduction, which is an important process in both Alpha Mound and Beta Mound, initially leads to undersaturation of calcium carbonate. However, both chemical modelling and field observations show that organoclastic sulphate reduction, upon continued bicarbonate addition and resulting increase in alkalinity, induces calcium carbonate oversaturation at later stages (Canfield & Raiswell, 1991; Sanders, 2003). Another consequence of sulphate reduction is the formation of iron sulphide mineral phases, which were found in high concentrations in Alpha Mound and Beta Mound sediments. This process not only acts as a sink for produced hydrogen sulphide (Tribble, 1993; Ku *et al.*, 1999), but further promotes carbonate precipitation. Early diagenetic processes steered by organoclastic sulphate reduction were already invoked to explain the formation of lithified carbonate layers

in other cold-water coral mounds (Pirlet *et al.*, 2010; Van der Land *et al.*, 2010).

The strongly negative $\delta^{13}C$ values of authigenic carbonates can be attributed to AOM (Mozley & Burns, 1993) because biogenic methane is commonly strongly depleted in ^{13}C. Precipitation of authigenic carbonates is favoured by AOM because this process efficiently increases pore water alkalinity (Ritger *et al.*, 1987; Aloisi *et al.*, 2000, 2002).

The comparably heavy carbon isotope composition of the bulk carbonate from layers within Alpha Mound and Beta Mound relative to methane-derived carbonate phases (<−25‰; Peckmann & Thiel, 2004) suggests that DIC for carbonate formation probably derived from a combination of DIC produced during AOM and organoclastic sulphate reduction close to the SMTZ. The hypothesis that AOM contributed to carbonate formation is supported by the heavy $\delta^{34}S$ values of the sedimentary pyrite at similar depths, which were attributed to sulphate reduction coupled to AOM at the depths of former SMTZs (Fig. 8) (Wehrmann *et al.*, 2010). Maignien *et al.* (2010) previously described the occurrence of AOM at shallow depths within Alpha Mound. Moreover, the focused precipitation of calcite in narrow zones argues for AOM because carbonate derived from organoclastic sulphate reduction is assumed to be distributed over a broad area of the sediment column (i.e. the sulphate-bearing sediment column; Paull & Ussler, 2008). The oxygen isotope composition of authigenic carbonates is controlled by a combination of factors including carbonate mineralogy and chemistry, temperature of precipitation and the oxygen isotopic composition of the interstitial water. In modern conditions, calcite, which precipitates in equilibrium with bottom sea water [$\delta^{18}O$ = 0·94‰ (VSMOW), T = 11°C, Craig & Gordon, 1965] will have a $\delta^{18}O$ value of +2·0‰ (VPDB) if the palaeothermometer of O'Neil *et al.* (1969) [$10^3 \ln\alpha = 2{\cdot}78 \times (10^6 T^{-2}) - 2{\cdot}89$, α = carbonate-water fractionation factor and T = bottom water temperature in Kelvin] is used. A $\delta^{18}O$ value of +2·8‰ (VPDB) is obtained according to the palaeothermometer of Tarutani *et al.* (1969) and Friedman & O'Neil (1977) for high-Mg calcite [$10^3 \ln\alpha = 2{\cdot}78 \times (10^6 T^{-2}) - 2{\cdot}89 + 0{\cdot}72$]. Calcite precipitation during glacial periods, characterized by cooler bottom waters, could easily produce $\delta^{18}O$ values exceeding +3‰ VPDB. Given that $\delta^{18}O$ values in the layers with calcite precipitation are between +2‰ and +2·9‰ (Fig. 7B), it might be concluded that the calcite precipitated in equilibrium with bottom sea water.

Dolomite

There is a significant difference between the dolomite content of Alpha Mound and Beta Mound. Beta Mound is characterized by a low dolomite content (3 to 5%) which correlates closely with the quartz and clay mineral contribution, suggesting a primarily detrital origin for these dolomites (Fig. 3). In addition, the observed dolomite crystals do not encrust biogenic fragments, as would be expected if they had a diagenetic origin. In contrast, Alpha Mound reveals a high amount of dolomite which constitutes up to 45% of the sediment (Fig. 2). These dolomite crystals have a diagenetic origin as numerous rhombs were observed which incorporate coccoliths and other biogenic fragments (Fig. 4A and B). Although dolomite occurs abundantly in the geological record, its formation in modern sediments remains uncertain (McKenzie, 1991). Several studies have linked dolomite formation to microbial organic matter degradation (Baker & Burns, 1985; Burns *et al.*, 1988; Compton, 1988) and especially the activity of sulphate reducers (Vasconcelos *et al.*, 1995; Vasconcelos & McKenzie, 1997; Wright, 1999; Van Lith *et al.*, 2003). Moore *et al.* (2004) and Meister *et al.* (2007) stated that dolomite forms preferentially at microbial hotspots such as the SMTZ where AOM results in the enhanced production of alkalinity. Based on the $\delta^{13}C$ value of the dolomite in Alpha Mound (−22·3‰), dolomite formation cannot be unequivocally attributed to AOM. It is likely that, similar to the described formation of authigenic calcite cements, dolomite precipitation in Alpha Mound occurred close to the SMTZ, where it incorporated DIC produced during AOM and organoclastic sulphate reduction. Furthermore, the isotope composition of the calcite ($\delta^{13}C$ = −12·5‰ and $\delta^{18}O$ = +2·4‰) associated with the dolomite shows that this calcite has a (partial) diagenetic origin as well (Fig. 7A). Overall, the low concentration of calcite in the dolomite layer may indicate that a significant part of the original carbonate was replaced by dolomite during a dolomitization process (Moore *et al.*, 2004). The parameters which control this dolomitization process remain uncertain. Possibly, authigenic calcite precipitated first and lowered the Ca-concentration in the pore water, thereby increasing the Mg/Ca ratio which favoured subsequent dolomitization. This requires a SMTZ which remains stable at a certain depth to sufficiently increase the Mg/Ca ratio.

The oxygen isotope composition of the dolomite in Alpha Mound indicates that dolomite precipitated from interstitial waters with a composition close to sea water with little or no brine influence. The $\delta^{18}O$ value of dolomite which precipitates in isotopic equilibrium with bottom sea water can be calculated with the palaeothermometer for microbial dolomite at low temperatures (Vasconcelos *et al.*, 2005) [$10^3 \ln\alpha = 2{\cdot}73 \times (10^6 \ T^{-2}) + 0{\cdot}26$]. Assuming a $\delta^{18}O_{SMOW}$ value for the bottom sea water of 0·94‰ and a temperature of 11°C (Craig & Gordon, 1965), dolomite with a $\delta^{18}O$ value of +4·6‰ (VPDB) is formed. This value is coherent with the $\delta^{18}O$ value of the dolomite (+4·8‰) in Alpha Mound (Fig. 7A). Moreover, the $\delta^{18}O$ value would be even higher if the dolomite was precipitated during glacial periods, when bottom waters were cooler. The finding that dolomite in Alpha Mound precipitated from interstitial waters with a composition close to sea water disagrees with the study of Wehrmann *et al.* (2010) who postulated the influence of a brine enriched in ^{18}O. The cause of the difference between these findings is rooted in the interpretation of the carbonate mineralogy (high-Mg calcite versus high-Ca dolomite) as the equilibrium isotope fractionation between dolomite and water is considerably larger than the corresponding isotope fractionation for high-Mg calcite. The study of Wehrmann *et al.* (2010) highlights the presence of high-Mg calcite in the coral mounds on Pen Duick Escarpment, whereas dolomite was reported to occur only in low quantities. In the present study however, only minor amounts of high-Mg calcite and a considerable high-Ca dolomite content were detected by XRD. It is assumed that the carbonate identified as 'high-Mg calcite' in Wehrmann *et al.* (2010) corresponds to the carbonate that is identified in the present study as 'high-Ca dolomite'. Strictly speaking, neither of the fractionation factors used in Wehrmann *et al.* (2010) and this study truly correspond to the isotope equilibrium between water and the observed carbonate mineral. Hence, the results of both studies have to be interpreted as end-member calculations.

Cold CL of the dolomite crystals reveals alternating dark and bright luminescent zones. This zonation indicates a change in the pore water chemistry which might be linked with alternating (sub)-oxic and reducing conditions controlling the concentration and oxidation state of Fe and Mn in the pore water (Richter *et al.*, 2003). Hence, the dolomite probably formed in different phases recording different redox conditions related to shifts in the location of the SMTZ. The alternation of (sub)-oxic and reducing conditions is probably also recorded in the isotopic values of the CAS extracted from a dolomite-rich sample, which may reflect the isotopic composition of pore water sulphate during dolomite formation. The $\delta^{18}O_{CAS}$ (+12·7‰) and $\delta^{34}S_{CAS}$ values (+21·7‰) of the dolomite reveal no significant enrichment compared to the isotopic value of sea water sulphate ($\delta^{18}O_{sea\ water}$ = +8·6‰ and $\delta^{34}S_{sea\ water}$ = +20·3‰; Longinelli, 1989) as would be expected if dolomite formed close to the SMTZ. However, it must be considered that dolomite forming close to the SMTZ cannot incorporate large amounts of sulphate because sulphate concentrations are low. It is probable that sulphate with an isotopic value close to sea water was incorporated during dolomite formation in a (sub)-oxic phase.

The role of the lithified layers

The occurrence of various lithified layers atop both Beta Mound and Alpha Mound as a result of the precipitation of authigenic minerals indicates that early diagenesis is an important and very active process in the stabilization of these mound structures. The lithified layers will stabilize the steep flanks of the mounds and form a protection against erosional processes. Indeed, exhumed rockslabs and firmgrounds have been observed on the coral mounds in Cadiz (Foubert *et al.*, 2008; Van Rooij *et al.*, 2010; De Mol *et al.*, in press) but also on the mounds off Ireland (Noé *et al.*, 2006; Wienberg *et al.*, 2008; de Haas *et al.*, 2009; Van der Land *et al.*, 2010).

The semi-lithified layers are characterized by poorly preserved aragonitic corals and other biogenic fragments (Fig. 6C to E). The mouldic shape of the pores indicates that aragonite dissolution occurred after or during carbonate precipitation, otherwise the moulds of the biogenic fragments would not have been preserved. It is probable that aragonite dissolution is the result of diffusing hydrogen sulphide, which acts as a weak acid (Soetaert *et al.*, 2007). This dissolution process occurs when all reactive iron in the sediment is consumed and no longer acts as a sink for the dissolved sulphide derived from sulphate reduction (Tribble, 1993; Ku *et al.*, 1999).

Dissolution and precipitation of carbonates also impacts the permeability of the coral mound and may strongly affect fluid pathways. The precipitation of calcite and dolomite results in a decrease of the permeability (Davis *et al.*, 2006) and,

therefore, the (semi)-lithified layers might act as a barrier for upward migrating fluids (Hovland, 2002; Naudts *et al.*, 2008). However, given that lithified layers are more prone to brittle deformation, processes such as sediment loading and hydrostatic pressure build-up (Conti *et al.*, 2004, 2008) may result in the brecciation which was observed in some of the layers of Alpha Mound and Beta Mound (Fig. 6C and E). Due to this brecciation, the lithified layers no longer act as a barrier and may even serve as pathways for fluid flow. Hence, diagenetic processes such as dissolution of aragonite, lithification by precipitation of authigenic minerals and subsequent brecciation of these lithified layers may affect advective and diffusive fluid flow within the mounds.

Early diagenesis in Alpha Mound versus Beta Mound

Alpha Mound and Beta Mound are located on the same escarpment, in a similar depth of water and separated by a lateral distance of 540 m (Fig. 1). Therefore, it can be assumed that these mounds received a similar sediment input and are influenced by the same water masses. Moreover, the major driver for diagenetic processes: organoclastic sulphate reduction and sulphate reduction coupled to AOM in the SMTZ is the same for both mounds. Nevertheless, Alpha Mound and Beta Mound are characterized by a different assemblage of authigenic minerals (Table 3) and, hence, diagenetic history. It is most likely that this heterogeneity between mounds can be attributed to differences in the intensity of sulphate reduction coupled to the AOM, to fluctuations in the position of the SMTZ and in the diffusive and advective fluid flow patterns in the mound.

Alpha Mound appears to have experienced higher methane fluxes than Beta Mound. This observation is corroborated by the extensive precipitation of dolomite depleted in ^{13}C, which requires a stable SMTZ with a strong production of alkalinity by AOM (Fig. 9). The high methane fluxes in Alpha Mound are also supported by the dominance of framboidal pyrite over euhedral pyrite, which is probably associated with extensive production of sulphide during sulphate reduction coupled to AOM. Alpha Mound was probably also more affected by shifts in the position of redox boundaries than Beta Mound. The zonation of the dolomite observed under CL indicates that dolomite precipitated in various episodes, which were probably characterized by varying redox conditions related to shifts in the position of the SMTZ (Fig. 9). Such a dynamic behaviour in the location of the SMTZ could be caused by episodic lateral inflow of sea water. This scenario was already postulated by Wehrmann *et al.* (2010) to explain the almost linear pore water sulphate profile in an adjacent core.

Sea water inflow could trigger the oxidation of sulphide minerals causing carbonate dissolution and the formation of authigenic gypsum crystals (Pirlet *et al.*, 2010) which were observed in Alpha Mound (Fig. 9). Other cores obtained from Alpha Mound lack such an influx in the pore water (Foubert *et al.*, 2008; Maignien *et al.*, 2010),

Table 3. Overview of the diagenetic features present in Alpha Mound and Beta Mound.

Diagenetic feature	Alpha Mound	Beta Mound
Framboidal pyrite	Large clusters throughout entire core	Minor quantities
Euhedral pyrite	Present in minor quantities as overgrowths on framboids	Large nodules up to ±1 cm throughout the entire core
Barite	Not present	Barite nodules in core catcher
Gypsum	Present in minor quantities at 101, 121 361 and 366 cm	Not present
Calcite	Present as overgrowths on coccoliths and intraparticular crystals in intervals: 367 to 375 cm and 419 to 445 cm	Present as overgrowths on coccoliths and intraparticular crystals in intervals: 101 to 120 cm, 234 to 268 cm, 281 to 300 cm and the core catcher
Dolomite	Present in large quantities in interval 162 to 255 cm and moderate to minor quantities in other parts of the core	Present in minor quantities
Mouldic porosity	162 to 255 cm, 367 to 375 cm and 419 to 445 cm	234 to 268 cm and 281 to 300 cm
Brecciation	419 to 445 cm	234 to 268 cm and 281 to 300 cm

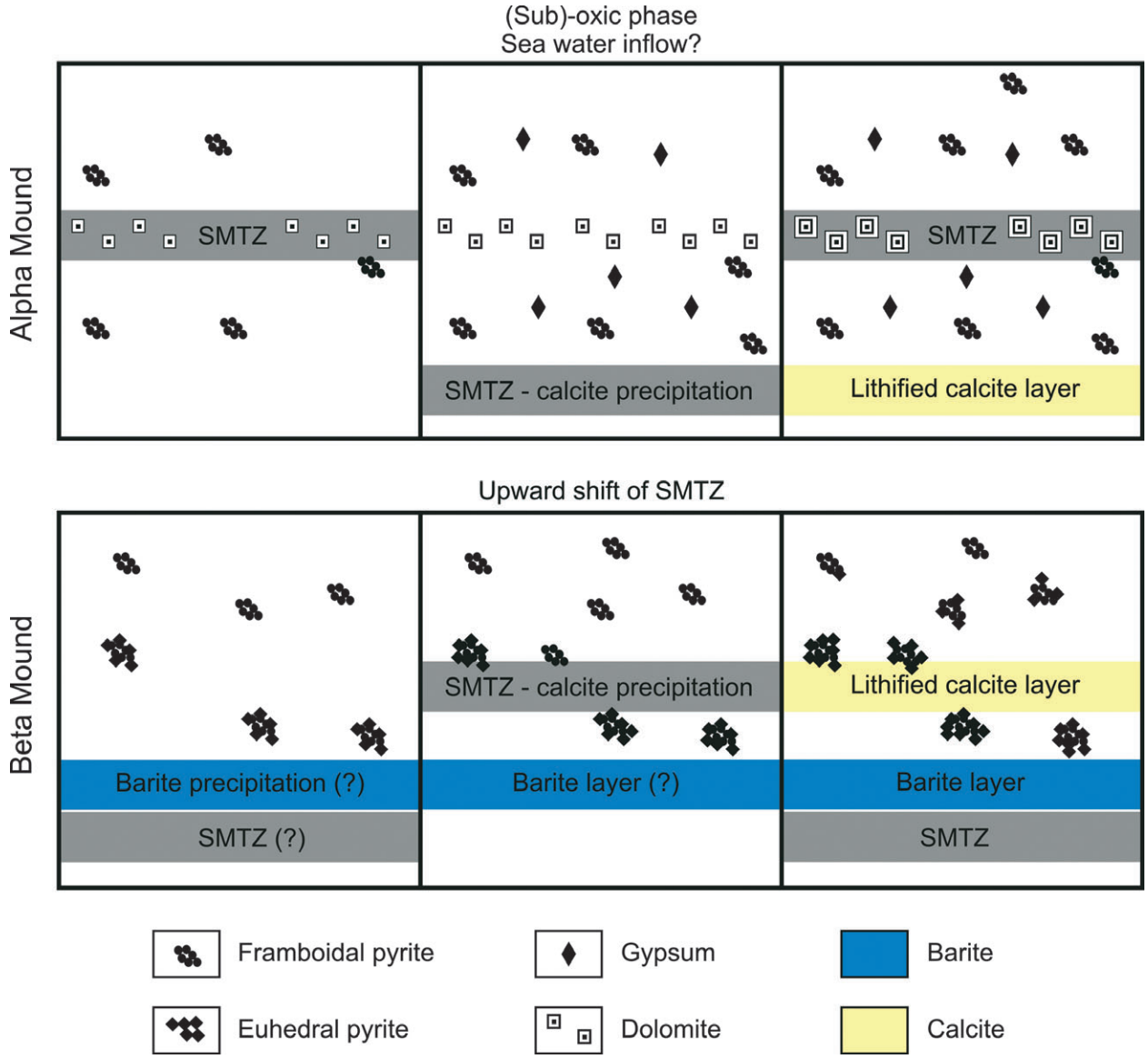

Fig. 9. Proposed models for the precipitation of the various authigenic minerals in Alpha Mound and Beta Mound tied to a shift in the position of the sulphate methane transition zone (SMTZ).

which may point to spatial and/or temporal differences in the sea water inflow. In this regard, the presence and spatial distribution of brecciated layers may be an important sedimentary feature as they may serve as a conduit for this sideward inflow. Depreiter (2009) proposed a pumping model where currents cause pressure gradients around obstacles on the sea bed which lead to the sideward inflow of sea water and a lowering of the SMTZ. In this context, Alpha Mound may be more prone to erosion events and sea water inflow due to its position, at the south-eastern edge of Pen Duick Escarpment.

In contrast to Alpha Mound, Beta Mound appears to be exposed to lower methane fluxes and a more static position of the SMTZ. The latter scenario with a stable position of the SMTZ for a longer period of time is supported by the precipitation of significant amounts of barite (Fig. 9; Torres *et al.*, 1996). In addition, the pore water data of Beta Mound also indicates that the current position of the SMTZ is below this barium-rich layer (Wehrmann *et al.*, 2010). Apparently, the flux of dissolved sulphide from this SMTZ is not as intense as for Alpha Mound. Under these conditions, formation of euhedral pyrite dominates. Nevertheless, there is also evidence for relocations of the SMTZ in Beta Mound to shallower depths, which led to the formation of calcite depleted in ^{13}C between 250 cm and

300 cm (Fig. 9). It is most likely that the SMTZ did not remain at this position for long enough to sufficiently increase the Mg/Ca ratio of the pore water to induce dolomite precipitation. However, the depletion of magnesium in the pore water with depth (Wehrmann *et al.*, 2010) indicates that dolomite is being formed at the present position of the SMTZ, below the barite layer.

CONCLUSIONS

The diagenetic processes in both Alpha Mound and Beta Mound are steered by organoclastic sulphate reduction and sulphate reduction coupled to anaerobic oxidation of methane (AOM) in a shallow sulphate methane transition zone (SMTZ). Nevertheless, both mounds reveal a specific assemblage of authigenic minerals: calcite, framboidal pyrite, gypsum and dolomite in Alpha Mound; and calcite, euhedral pyrite and barite in Beta Mound. These assemblages point to different diagenetic histories which may be attributed to variations in the intensity of sulphate reduction coupled to AOM, in the dynamics of the fluctuations in the depth of the SMTZ and in the diffusive and advective fluid flow patterns in the mound.

In this regard, the sedimentary diagenetic features of the mounds also affect the advection and diffusion of dissolved compounds, thereby influencing the ongoing diagenetic processes. Generation of secondary porosity by the dissolution of aragonite, for example, may contribute to an enhanced flux of methane, promoting subsequent lithification by precipitation of authigenic minerals which, in turn, may reduce the overall permeability of the sediment. The formation of lithified layers contributes to the stabilization of the mounds, but also forms layers that are susceptible to brittle deformation, opening pathways for subsequent fluid migration and thus amplifying the dynamics of the entire diagenetic system. Hence, the cold-water coral mounds from the Pen Duick Escarpment are not just the result of coral growth, subsequent sediment infill and the shaping by currents, but also an expression of their internal diagenetic dynamics.

The findings of this study demonstrate that early diagenetic processes may induce significant differences between sedimentary records which are situated in identical sedimentological and oceanographic settings. Moreover, these early diagenetic differences will probably result in additional differences with continued burial, which has implications for studying such mounds in the geological record.

ACKNOWLEDGEMENTS

The authors would like to acknowledge the captain, crew and shipboard party of *R/V Marion Dufresne* (2008). We especially want to thank IPEV, Y. Balut, H. Leau and Y. Reaud for the logistical and operational support for the coring facilities during MD140 and MD169. The MD169 MiCROSYSTEMS cruise was financially supported by the CNRS-EDD. B. Delay (Scientific Board) and N. Gibelin (International relations) are warmly thanked for their active contribution to this project. DB and the LSCE scientists wish to thank the CEA for its support. We express our thanks to H. Nijs for preparing the thin sections and D. Steeno for technical assistance during the cathodoluminescence work. The authors would also like to thank Henri Houbrechts (Ghent University Hospital) for his help with the medical CT scanning. This study was conducted within the framework of the ESF EuroDIVERSITY MiCROSYSTEMS project. H. Pirlet and V. Cnudde are currently funded by the Fund for Scientific Research – Flanders (FWO – Vlaanderen). The Institute for the Promotion of Innovation through Science and Technology in Flanders (IWT-Vlaanderen) is acknowledged for its grant to J. Dewanckele and L. De Mol. The editor and two anonymous reviewers are thanked for their helpful comments and suggestions which improved the manuscript considerably.

REFERENCES

Aloisi, G., Pierre, C., Rouchy, J.M., Foucher, J.P., Woodside, J. and **Party, M.S.** (2000) Methane-related authigenic carbonates of eastern Mediterranean Sea mud volcanoes and their possible relation to gas hydrate destabilisation. *Earth Planet. Sci. Lett.*, **184,** 321–338.

Aloisi, G., Bouloubassi, I., Heijs, S.K., Pancost, R.D., Pierre, C., Damste, J.S.S., Gottschal, J.C., Forney, L.J. and **Rouchy, J.M.** (2002) CH4-consuming microorganisms and the formation of carbonate crusts at cold seeps. *Earth Planet. Sci. Lett.*, **203,** 195–203.

Aloisi, G., Wallmann, K., Bollwerk, S.M., Derkachev, A., Bohrmann, G. and **Suess, E.** (2004) The effect of dissolved barium on biogeochemical processes at cold seeps. *Geochim. Cosmochim. Acta*, **68,** 1735–1748.

Baker, P.A. and **Burns, S.J.** (1985) Occurence and formation of dolomite in organic-rich continental margin sediments. *AAPG Bull.*, **69,** 1917–1930.

Berastegui, X., Banks, C.J., Puig, C., Taberner, C., Waltham, D. and **Fernandez, M.** (1998) Lateral diapiric emplacement of

Triassic evaporites at the southern margin of Guadalquivir Basin, Spain. In: *Cenozoic Foreland Basins of Western Europe* (Ed. A. Mascle), *Geol. Soc. Spec. Publ.*, 49–68.

Berner, R.A. (1970) Sedimentary pyrite formation. *Am. J. Sci.*, **268,** 1–23.

Burns, S.J., Baker, P.A. and **Showers, W.J.** (1988) The factors controlling the formation and chemistry of dolomite in organic-rich sediments: Miocene Drakes Bay Formation, California. In: *Sedimentology and Geochemistry of Dolostones* (Eds V. Shukla and P.A. Baker), *SEPM Spec. Publ.*, **43,** 3–10.

Canfield, D.E. and **Raiswell, R.** (1991) Carbonate precipitation and dissolution. In: *Taphonomy. Releasing the Data Locked in the Fossil Record* (Eds P.A. Allison and D.E.G. Briggs), pp. 411–453. Plenum Press, New York.

Caralp, M.H. (1988) Late glacial to recent deep-sea benthic foraminifera from the Northeastern Atlantic (Cadiz Gulf) and Western Mediterranean (Alboran Sea): paleoceanographic results. *Mar. Micropaleontol.*, **13,** 265–289.

Castellini, D.G., Dickens, G.R., Snyder, G.T. and **Ruppel, C.D.** (2006) Barium cycling in shallow sediment above active mud volcanoes in the Gulf of Mexico. *Chem. Geol.*, **226,** 1–30.

Compton, J.S. (1988) Sediment composition and precipitation of dolomite and pyrite in the Neogene Monterey and Sisquoc Formations, Santa Maria Basin area, California. In: *Sedimentology and Geochemistry of Dolostones* (Eds V. Shukla and P.A. Baker), *SEPM Spec. Publ.*, **43,** 53–64.

Conti, S., Fontana, D., Gubertini, A., Sighinolfi, G., Tateo, F., Fioroni, C. and **Fregni, P.** (2004) A multidisciplinary study of middle Miocene seep-carbonates from the northern Apennine foredeep (Italy). *Sed. Geol.*, **169,** 1–19.

Conti, S., Fontana, D. and **Lucente, C.C.** (2008) Authigenic seep-carbonates cementing coarse-grained deposits in a fan-delta depositional system (middle Miocene, Marnoso-arenacea Formation, central Italy). *Sedimentology*, **55,** 471–486.

Craig, H. and **Gordon, L.I.** (1965) Deuterium and oxygen-18 variations in the ocean and marine atmosphere. In: *Stable Isotopes in Oceanic Studies and Paleotemperatures* (Ed. E. Tongiori), pp. 9–130. Consiglio Nazionale Delle Ricerche, Laboratorio di Geologia Nucleare, Pisa.

Curtis, C.D., Petrowski, C. and **Oertel, G.** (1972) Stable carbon isotope ratios within carbonate concretions: a clue to the place and time of formation. *Nature*, **235,** 98–100.

Davis, J.M., Roy, N.D., Mozley, P.S. and **Hall, J.S.** (2006) The effect of carbonate cementation on permeability heterogeneity in fluvial aquifers: an outcrop analog study. *Sed. Geol.*, **184,** 267–280.

De Mol, B., Van Rensbergen, P., Pillen, S., Van Herreweghe, K., Van Rooij, D., McDonnell, A., Huvenne, V., Ivanov, M., Swennen, R. and **Henriet, J.-P.** (2002) Large deep-water coral banks in the Porcupine Basin, southwest of Ireland. *Mar. Geol.*, **188,** 193–231.

De Mol, L., Hilário, A., Van Rooij, D. and **Henriet, J.-P.** (in press) Habitat mapping of a cold-water coral mound on Pen Duick Escarpment (Gulf of Cadiz). In: *Seafloor Geomorphology as Benthic Habitat: GeoHab Atlas of Seafloor Geomorphic Features and Benthic Habitats* (Eds P. Harris and E. Baker). Elsevier E-book publications, London.

Depreiter, D. (2009) *Sources, modes and effects of seabed fluid flow*. PhD, Ghent University, Ghent, 207 pp.

Dickens, G.R. (2001) Sulfate profiles and barium fronts in sediment on the Blake Ridge: present and past methane fluxes through a large gas hydrate reservoir. *Geochim. Cosmochim. Acta*, **65,** 529–543.

Ferdelman, T.G., Kano, A., Williams, T., Henriet, J.P. and **Scientists, I.E.** (2006) IODP Expedition 307 drills cold-water coral mound along the Irish continental margin. *Sci. Drilling*, **2,** 11–16.

Fossing, H. and **Jorgensen, B.B.** (1989) Measurement of bacterial sulfate reduction in sediments – evaluation of a single-step chromium reduction method. *Biogeochemistry*, **8,** 205–222.

Foubert, A. and **Henriet, J.P.** (2009) *Nature and Significance of the Recent Carbonate Mound Record: the Mound Challenger Code*. Springer-Verlag, Heidelberg, 350 pp.

Foubert, A., Depreiter, D., Beck, T., Maignien, L., Pannemans, B., Frank, N., Blamart, D. and **Henriet, J.-P.** (2008) Carbonate mounds in a mud volcano province off north-west Morocco: key to processes and controls. *Mar. Geol.*, **248,** 74–96.

Friedman, I. and **O'Neil, J.R.** (1977) Compilation of stable isotope fractionation factors of geochemical interest. In: *Data of Geochemistry* (Ed. M. Fleischer), *US Geol. Surv.*, **440 KK,** 1–12. Professional Paper

Goldhaber, M.B. and **Kaplan, I.R.** (1980) Mechanisms of sulfur incorporation and isotope fractionation during early diagenesis in sediments of the Gulf of California. *Mar. Chem.*, **9,** 95–143.

Greinert, J., Bollwerk, S.M., Derkachev, A., Bohrmann, G. and **Suess, E.** (2002) Massive barite deposits and carbonate mineralization in the Derugin Basin, Sea of Okhotsk: precipitation processes at cold seep sites. *Earth Planet. Sci. Lett.*, **203,** 165–180.

Gutscher, M.A., Malod, J., Rehault, J.P., Contrucci, I., Klingelhoefer, F., Mendes-Victor, L. and **Spakman, W.** (2002) Evidence for active subduction beneath Gibraltar. *Geology*, **30,** 1071–1074.

de Haas, H., Mienis, F., Frank, N., Richter, T.O., Steinacher, R., De Stigter, H., van der Land, C. and **Van Weering, T.C.E.** (2009) Morphology and sedimentology of (clustered) cold-water coral mounds at the south Rockall Trough margins, NE Atlantic Ocean. *Facies*, **55,** 1–26.

Henriet, J.-P., De Mol, B., Pillen, S., Vanneste, M., Van Rooij, D., Versteeg, W., Croker, P.F., Shannon, P.M., Unnithan, V., Bouriak, S., Chachkine, P. and **The Porcupine-Belgica 97 Shipboard Party** (1998) Gas hydrate crystals may help build reefs. *Nature*, **391,** 648–649.

Hensen, C., Nuzzo, M., Hornibrook, E., Pinheiro, L.M., Bock, B., Magalhaes, V.H. and **Bruckmann, W.** (2007) Sources of mud volcano fluids in the Gulf of Cadiz – indications for hydrothermal imprint. *Geochim. Cosmochim. Acta*, **71,** 1232–1248.

Hovland, M. (2002) On the self-sealing nature of marine seeps. *Cont. Shelf Res.*, **22,** 2387–2394.

Iorga, M.C. and **Lozier, M.S.** (1999) Signatures of the Mediterranean outflow from a North Atlantic climatology 1. Salinity and density fields. *J. Geophys. Res.-Oceans*, **104,** 25985–26009.

Jørgensen, B.B., Böttcher, M.E., Luschen, H., Neretin, L.N. and **Volkov, I.I.** (2004) Anaerobic methane oxidation and a deep H_2S sink generate isotopically heavy sulfides in Black Sea sediments. *Geochim. Cosmochim. Acta*, **68,** 2095–2118.

Kak, A.C. and **Slaney, M.** (1988) *Principles of Computerized Tomographic Imaging*. IEEE press, New York, 344 pp.

Kano, A., Ferdelman, T.G., Williams, T., Henriet, J.P., Ishikawa, T., Kawagoe, N., Takashima, C., Kakizaki, Y., Abe, K., Sakai, S., Browning, E., Li, X. and **the IODP Expedition 307 Scientists** (2007) Age constraints on the origin and growth history of a deep-water coral mound in northeast Atlantic drilled during Integrated Ocean Drilling Program Expedition 307. *Geology*, **35,** 1051–1054.

Kenyon, N.H., Akhmetzhanov, A.M., Wheeler, A.J., van Weering, T.C.E., de Haas, H. and **Ivanov, M.K.** (2003) Giant carbonate mud mounds in the southern Rockall Trough. *Mar. Geol.*, **195,** 5–30.

Ku, T.C.W., Walter, L.M., Coleman, M.L., Blake, R.E. and **Martini, A.M.** (1999) Coupling between sulfur recycling and syndepositional carbonate dissolution: evidence from oxygen and sulfur isotope composition of pore water sulfate, South Florida Platform, USA. *Geochim. Cosmochim. Acta*, **63,** 2529–2546.

Longinelli, A. (1989) Oxygen-18 and sulphur-34 in dissolved oceanic sulphate and phosphate. In: *Handbook of Environmental Isotope Geochemistry* (Eds P. Fritz and J.C. Fontes), **3**, pp. 219–255. Elsevier, Amsterdam.

Machin, F., Pelegri, J.L., Marrero-Diaz, A., Laiz, I. and **Ratsimandresey, A.** (2006) Near-surface circulation in the southern Gulf of Cadiz. *Deep Sea Res. Part II: Topical Stud. Oceanogr.*, **63,** 1161–1181.

Maestro, A., Somoza, L., Medialdea, T., Talbot, C.J., Lowrie, A., Vazquez, J.T. and **Diaz-del-Rio, V.** (2003) Large-scale slope failure involving Triassic and Middle Miocene salt and shale in the Gulf of Cadiz (Atlantic Iberian Margin). *Terra Nova*, **15,** 380–391.

Maignien, L., Depreiter, D., Foubert, A., Reveillaud, J., De Mol, L., Boeckx, P., Blamart, D., Henriet, J.P. and **Boon, N.** (2010) Anaerobic oxidation of methane in a cold-water coral carbonate mound from the Gulf of Cadiz. *Int. J. Earth Sci. (Geol. Rundsch.)*. doi: 10.1007/s00531-010-0528-z.

Maldonado, A., Somoza, L. and **Pallares, L.** (1999) The Betic orogen and the Iberian-African boundary in the Gulf of Cadiz: geological evolution (central North Atlantic). *Mar. Geol.*, **155,** 9–43.

Malone, M.J., Baker, P.A. and **Burns, S.J.** (1994) Recrystallization of dolomite: evidence from the Monterey Formation (Miocene), California. *Sedimentology*, **41,** 1223–1239.

Marshall, J.D. (1988) *Cathodoluminescence of Geological Materials*. Unwin Hyman, Boston, 146 pp.

Masschaele, B.C., Cnudde, V., Dierick, M., Jacobs, P., Van Hoorebeke, L. and **Vlassenbroeck, J.** (2007) UGCT: new x-ray radiography and tomography facility. *Nucl. Instrum. Methods Phys. Res., Sect, A*, **580,** 266–269.

McKenzie, J.A. (1991) The dolomite problem: an outstanding controversy. In: *Controversies in Modern Geology* (Eds D.W. Müller, J.A. McKenzie and H. Weissert), pp. 35–54. Academic Press, London.

Medialdea, T., Vegas, R., Somoza, L., Vazquez, J.T., Maldonado, A., Diaz-Del-Rio, V., Maestro, A., Cordoba, D. and **Fernandez-Puga, M.C.** (2004) Structure and evolution of the ''Olistostrome'' complex of the Gibraltar Arc in the Gulf of Cadiz (eastern Central Atlantic): evidence from two long seismic cross-sections. *Mar. Geol.*, **209,** 173–198.

Meister, P., Mckenzie, J.A., Vasconcelos, C., Bernasconi, S., Frank, M., Gutjahr, M. and **Schrag, D.P.** (2007) Dolomite formation in the dynamic deep biosphere: results from the Peru Margin. *Sedimentology*, **54,** 1007–1031.

Merinero, R., Lunar, R., Martinez-Fiias, J., Somoza, L. and **Diaz-del-Rio, V.** (2008) Iron oxyhydroxide and sulphide mineralization in hydrocarbon seep-related carbonate submarine chimneys, Gulf of Cadiz (SW Iberian Peninsula). *Mar. Petrol. Geol.*, **25,** 706–713.

Moore, T.S., Murray, R.W., Kurtz, A.C. and **Schrag, D.P.** (2004) Anaerobic methane oxidation and the formation of dolomite. *Earth Planet. Sci. Lett.*, **229,** 141–154.

Morse, J.W. (2003) Formation and diagenesis of carbonate sediments. In: *Sediments, Diagenesis and Sedimentary Rocks* (Ed. F.T. Mackenzie), *Treatise on Geochem.*, **7,** 67–86.

Mozley, P.S. and **Burns, S.J.** (1993) Oxygen and carbon isotopic composition of marine carbonate concretions – an overview. *J. Sed. Petrol.*, **63,** 73–83.

Naudts, L., Greinert, J., Artemov, Y., Beaubien, S.E., Borowski, C. and **De Batist, M.** (2008) Anomalous sea-floor backscatter patterns in methane venting areas, Dnepr paleodelta, NW Black Sea. *Mar. Geol.*, **251,** 253–267.

Neretin, L.N., Böttcher, M.E., Jørgensen, B.B., Volkov, I.I., Luschen, H. and **Hilgenfeldt, K.** (2004) Pyritization processes and greigite formation in the advancing sulfidization front in the Upper Pleistocene sediments of the Black Sea. *Geochim. Cosmochim. Acta*, **68,** 2081–2093.

Noé, S., Titschack, J., Freiwald, A. and **Dullo, W.C.** (2006) From sediment to rock: diagenetic processes of hardground formation in deep-water carbonate mounds of the NE Atlantic. *Facies*, **52,** 183–208.

Ohfuji, H. and **Rickard, D.** (2005) Experimental syntheses of framboids – a review. *Earth-Sci. Rev.*, **71,** 147–170.

O'Neil, J.R., Clayton, R.N. and **Mayeda, T.K.** (1969) Oxygen isotope fractionation in divalent metal carbonates. *J. Chem. Phys.*, **51,** 5547–5558.

Passier, H.F., Middelburg, J.J., deLange, G.J. and **Bottcher, M.E.** (1997) Pyrite contents, microtextures, and sulfur isotopes in relation to formation of the youngest eastern Mediterranean sapropel. *Geology*, **25,** 519–522.

Passier, H.F., Middelburg, J.J., de Lange, G.J. and **Bottcher, M.E.** (1999) Modes of sapropel formation in the eastern Mediterranean: some constraints based on pyrite properties. *Mar. Geol.*, **153,** 199–219.

Paull, C.K. and **Ussler, W. III** (2008) Re-evaluating the significance of seafloor accumulations of methane-derived carbonates: seepage or erosion indicators? In: Proceedings of the 6th International Conference on Gas Hydrates (ICGH 2008), Vancouver, British Columbia, Canada.

Paytan, A. and **Griffith, E.M.** (2007) Marine barite: recorder of variations in ocean export productivity. *Deep-Sea Res. Part II-Topical Stud. Oceanogr.*, **54,** 687–705.

Peckmann, J. and **Thiel, V.** (2004) Carbon cycling at ancient methane-seeps. *Chem. Geol.*, **205,** 443–467.

Pelegri, J.L., Aristegui, J., Cana, L., Gonzalez-Davila, M., Hernandez-Guerra, A., Hernandez-Leon, S., Marrero-Diaz, A., Montero, M.F., Sangra, P. and **Santana-Casiano, M.** (2005) Coupling between the open ocean and the coastal upwellng region off northwest Africa: water recirculation and offshore pumping of organic matter. *J. Mar. Syst.*, **54,** 3–37.

Pinheiro, L., Ivanov, M.K., Sautkin, A., Akhmanov, G., Magalhaes, V., Volkonskaya, A., Monteiro, J.H., Somoza, L., Gardner, J., Hamouni, N. and **Cunha, M.R.** (2004) Mud volcanism in the Gulf of Cadiz: results from the TTR-10 cruise. *Mar. Geol.*, **195,** 131–151.

Pirlet, H., Wehrmann, L.M., Brunner, B., Frank, N., Dewanckele, J., Van Rooij, D., Foubert, A., Swennen, R., Naudts, L., Boone, M., Cnudde, V. and **Henriet, J.P.** (2010) Diagenetic formation of gypsum and dolomite in a cold-water coral mound in the Porcupine Seabight, off Ireland. *Sedimentology*, **57,** 786–805.

Pisciotto, K.A. and **Mahoney, J.J.** (1981) Isoptopic survey of diagenetic carbonates, DSDP leg 63. *Init. Rep. Deep Sea Drilling Proj.*, **63,** 595–609.

Raiswell, R. (1982) Pyrite texture, isotopic composition and the availability of iron. *Am. J. Sci.*, **282,** 1244–1263.

Richter, D.K., Gotte, T., Gotze, J. and **Neuser, R.D.** (2003) Progress in application of cathodoluminescence (CL) in sedimentary petrology. *Mineral. Petrol.*, **79,** 127–166.

Riedinger, N., Kasten, S., Groger, J., Franke, C. and **Pfeifer, K.** (2006) Active and buried authigenic barite fronts in sediments from the Eastern Cape Basin. *Earth Planet. Sci. Lett.*, **241,** 876–887.

Ritger, S., Carson, B. and **Suess, E.** (1987) Methane-derived authigenic carbonates formed by subduction induced pore-water expulsion along the Oregon Washington margin. *Geol. Soc. Am. Bull.*, **98,** 147–156.

Roberts, J.M., Wheeler, A.J. and **Freiwald, A.** (2006) Reefs of the deep: the biology and geology of cold-water coral ecosystems. *Science*, **312,** 543–547.

Rosenbaum, J. and **Sheppard, S.M.F.** (1986) An isotopic study of siderites, dolomites and ankerites at high-temperatures. *Geochim. Cosmochim. Acta*, **50,** 1147–1150.

Sanders, D. (2003) Syndepositional dissolution of calcium carbonate in neritic carbonate environments: geological recognition, processes, potential significance. *J. Afr. Earth Sci.*, **36,** 99–134.

Sartori, R., Torelli, L., Zitellini, N., Peis, D. and **Lodolo, E.** (1994) Eastern segment of the Azores-Gibraltar line (central-eastern Atlantic) – an oceanic plate boundary with diffuse compressional deformation. *Geology*, **22,** 555–558.

Snyder, G.T., Dickens, G.R. and **Castellini, D.G.** (2007) Labile barite contents and dissolved barium concentrations on Blake Ridge: new perspectives on barium cycling above gas hydrate systems. *J. Geochem. Explor.*, **95,** 48–65.

Soetaert, K., Hofmann, A.F., Middelburg, J.J., Meysman, F.J.R. and **Greenwood, J.** (2007) The effect of biogeochemical processes on pH. *Mar. Chem.*, **105,** 30–51.

Somoza, L., Diaz-del Rio, V., Leon, R., Ivanov, M.K., Fernandez-Puga, M.C., Gardner, J., Hernandez-Molina, F.J., Pinheiro, L., Rodero, J., Lobato, A., Maestro, A., Vazquez, J.T., Medialdea, T. and **Fernandez-Salas, L.M.** (2003) Seabed morphology and hydrocarbon seepage in the Gulf of Cadiz mud volcano area: acoustic imagery, multibeam and ultra-high resolution seismic data. *Mar. Geol.*, **195,** 153–176.

Sweeney, R.E. and **Kaplan, I.R.** (1973) Pyrite framboid formation – laboratory synthesis and marine sediments. *Econ. Geol.*, **68,** 618–634.

Tarutani, T., Clayton, R.N. and **Mayeda, T.K.** (1969) Effect of polymorphism and magnesium substitution on oxygen isotope fractionation between calcium carbonate and water. *Geochim. Cosmochim. Acta*, **33,** 987–996.

Torres, M.E., Brumsack, H.J., Bohrmann, G. and **Emeis, K.C.** (1996) Barite fronts in continental margin sediments: a new look at barium remobilization in the zone of sulfate reduction and formation of heavy barites in diagenetic fronts. *Chem. Geol.*, **127,** 125–139.

Torres, M.E., Bohrmann, G., Dube, T.E. and **Poole, F.G.** (2003) Formation of modern and Paleozoic stratiform barite at cold methane seeps on continental margins. *Geology*, **31,** 897–900.

Tribble, G.W. (1993) Organic-matter oxidation and aragonite diagenesis in a coral-reef. *J. Sed. Petrol.*, **63,** 523–527.

Van der Land, C., Mienis, F., De Haas, H., Frank, N., Swennen, R. and **Van Weering, T.C.E.** (2010) Diagenetic processes in carbonate mound sediments at the southwest Rockall Trough margin. *Sedimentology*, **57,** 912–931.

Van Lith, Y., Warthmann, R., Vasconcelos, C. and **Mckenzie, J.A.** (2003) Sulphate-reducing bacteria induce low-temperature Ca-dolomite and high Mg-calcite formation. *Geobiology*, **1,** 71–79.

Van Rensbergen, P., Depreiter, D., Pannemans, B., Moerkerke, G., Van Rooij, D., Marsset, B., Akhmanov, G., Blinova, V., Ivanov, M.K., Rachidi, M., Magalhaes, V., Pinheiro, L. and **Henriet, J.-P.** (2005) The El Arraiche mud volcano field at the Moroccan Atlantic slope, Gulf of Cadiz. *Mar. Geol.*, **219,** 1–17.

Van Rooij, D., Blamart, D., De Mol, L., Mienis, F., Pirlet, H., Wehrmann, L.M., Maignien, L., Templer, S.P., De Haas, H., Barbieri, R., Hebbeln, D., Frank, N., Larmagnat, S., Stadnitskaia, A., Stivaletta, N., Van Weering, T.C.E., Zhang, Y., Hamoumi, N., Duyck, P., Henriet, J.P. and **Party, T.M.M.S.** (2010) Cold-water coral mounds on the Pen Duick Escarpment, Gulf of Cadiz: the MiCROSYSTEMS approach. *Mar. Geol.*, **282,** 102–117.

Vasconcelos, C. and **McKenzie, J.A.** (1997) Microbial mediation of modern dolomite precipitation and diagenesis under anoxic conditions (Lagoa Vermelha, Rio de Janeiro, Brazil). *J. Sed. Res.*, **67,** 378–390.

Vasconcelos, C., Mckenzie, J.A., Bernasconi, S., Grujic, D. and **Tien, A.J.** (1995) Microbial mediation as a possible mechanism for natural dolomite formation at low-temperatures. *Nature*, **377,** 220–222.

Vasconcelos, C., McKenzie, J.A., Warthmann, R. and **Bernasconi, S.M.** (2005) Calibration of the delta O-18 paleothermometer for dolomite precipitated in microbial cultures and natural environments. *Geology*, **33,** 317–320.

Vlassenbroeck, J., Dierick, M., Masschaele, B., Cnudde, V., Hoorebeke, L. and **Jacobs, P.** (2007) Software tools for quantification of X-ray microtomography. *Nucl. Instrum. Meth. Phys. Res. Section a-Accelerators Spectrometers Detectors and Associated Equipment*, **580,** 442–445.

Wachter, E.A. and **Hayes, J.M.** (1985) Exchange of oxygen isotopes in carbon dioxide-phosphoric acid systems. *Chem. Geol.*, **52,** 365–374.

Webster, G., Blazejak, A., Cragg, B.A., Schippers, A., Sass, H., Rinna, J., Tang, X., Mathes, F., Ferdelman, T.G., Fry, J.C., Weightman, A.J. and **Parkes, R.J.** (2008) Subsurface microbiology and biogeochemistry of a deep, cold-water carbonate mound from the Porcupine Seabight (IODP Expedtion 307). *Environ. Microbiol.*, **11,** 239–257.

van Weering, T.C.E., de Haas, H., Akhmetzhanov, A.M. and **Kenyon, N.H.** (2003) Giant carbonate mounds along the Porcupine and SW Rockall Trough margins. In: *European Margin Sediment Dynamics: Side-Scan Sonar and Seismic Images* (Eds J. Mienert and P.P.E. Weaver), pp. 211–216. Springer-Verlag, Heidelberg.

Wehrmann, L.M., Knab, N.J., Pirlet, H., Unnithan, V., Wild, C. and **Ferdelman, T.G.** (2009) Carbon mineralization and carbonate preservation in modern cold-water coral reef sediments on the Norwegian shelf. *Biogeosciences*, **6,** 663–680.

Wehrmann, L.M., Templer, S.P., Brunner, B., Bernasconi, S.M., Maignien, L. and **Ferdelman, T.G.** (2010) The imprint of methane seepage on the geochemical record and early diagenetic processes in cold-water coral mounds on Pen Duick Escarpment, Gulf of Cadiz. *Mar. Geol.*, **282,** 118–137.

Wienberg, C., Beuck, L., Heidkamp, S., Hebbeln, D., Freiwald, A., Pfannkuche, O. and **Monteys, X.** (2008) Franken Mound: facies and biocoenoses on a newly-discovered ''carbonate mound'' on the western Rockall Bank, NE Atlantic. *Facies*, **54,** 1–24.

Wienberg, C., Hebbeln, D., Fink, H.G., Mienis, F., Dorschel, B., Vertino, A., Correa, M.L. and **Freiwald, A.** (2009) Scleractinian cold-water corals in the Gulf of Cadiz-First clues

about their spatial and temporal distribution. *Deep-Sea Res. Part I-Oceanogr. Res. Pap.*, **56,** 1873–1893.

Wright, D.T. (1999) The role of sulphate-reducing bacteria and cyanobacteria in dolomite formation in distal ephemeral lakes of the Coorong region, South Australia. *Sed. Geol.*, **126,** 147–157.

Zitellini, N., Gracia, E., Matias, L., Terrinha, P., Abreu, M.A., DeAlteriis, G., Henriet, J.P., Danobeitia, J.J., Masson, D.G., Mulder, T., Ramella, R., Somoza, L. and **Diez, S.** (2009) The quest for the Africa-Eurasia plate boundary west of the Strait of Gibraltar. *Earth Planet. Sci. Lett.*, **280,** 13–50.

Manuscript received 8 September 2010; revision accepted 20 May 2011